PolarGap 2015/16

Filling the GOCE polar gap in Antarctica and ASIRAS flight around South Pole

FINAL REPORT

Rene Forsberg, Arne V Olesen, DTU-Space
Fausto Ferraccioli, Tom Jordan, Hugh Corr, BAS
Kenichi Matsuoka, NPI
Dec 2017

ESA STUDY CONTRACT REPORT

SA CONTRACT NO 4000115220/15/NL/gp	**SUBJECT** Technical Support for the 2015/16 Airborne Polar Gap Campaign in Antarctica		**CONTRACTOR** NERC-British Antarctic Survey
ESA CR No	**STAR CODE**	**No of volumes** 1 **This is Volume No** 1	**CONTRACTORS REFERENCE** PolarGap 2015/16

ABSTRACT

This report describes the results of the ESA PolarGap airborne gravity, lidar/radar and aeromagnetic survey, carried out in Antarctica in the field season 2015/16. The primary aim of PolarGAP was to fill in the GOCE southern polar gap with new high-quality airborne gravity data, and the associated estimation of gravity gradients at altitude, as well as collecting Ku-band radar data (ASIRAS) in a smaller area at the southern limits of the CryoSat orbit, to get data on radar penetration into the snow and firn, in order to improve understanding of apparent anomalies in elevation changes in the region. In addition, aeromagnetic and ice-penetrating radar data were collected on an opportunistic basis, providing additional datasets of relevance to the SWARM mission and augmenting continental scale compilations such as BEDMAP 2 and ADMAP 2.

The PolarGap 2015/16 survey was a major success, with nearly 100% of planned data acquired, relative to the campaign implementation plan. The campaign was – in addition to ESA – supported by in-kind contributions of the British Antarctic Survey, DTU Space, the Norwegian Polar Institute, as well as the US National Science Foundation, the latter providing access and fuel at Amundsen-Scott South Pole Station, a key logistics element for successfully accomplishing the mission goals.

This report outlines the data processing, quality assessment, and data formats of the final data delivered to the ESA campaigns office. Together with the earlier "PolarGap 2015/16 Data Acquisition Report" these documents provide the full documentation for the PolarGap survey.

The work described in this report was done under ESA Contract. Responsibility for the contents resides in the author or organisation that prepared it.

Names of authors:

Rene Forsberg, Arne V Olesen, Fausto Ferraccioli, Tom Jordan, Hugh Corr, Kenichi Matsuoka

NAME OF ESA STUDY MANAGER	**ESA BUDGET HEADING**
Tania Casal Mission Science Division Validation Campaigns – ESTEC	

TABLE OF CONTENTS

1. INTRODUCTION

The ESA PolarGap gravity field campaign was successfully carried out in the period DEC 7, 2015 – JAN 19, 2016, where a suite of geophysical data (gravity, magnetic, ice-penetrating radar and scanning lidar) was successfully collected from a BAS Twin-Otter aircraft. As a consequence of the PolarGap Airborne Survey, the last and most challenging data gap in Antarctica is now covered with reconnaissance airborne geophysical data, and the last remaining data void on the planet filled with medium-resolution gravity data.

The details of the field surveys are described in the document [RD1]: "PolarGap 2015/16: Filling the GOCE Polar Gap in Antarctica, Data Acquisition Report", version 4, submitted to ESA, June 2016.

The primary objective of the PolarGap campaign was to carry out an airborne gravity survey covering the southern polar gap of the ESA gravity field mission GOCE, beyond the coverage of the GOCE orbit (south of 83.5°S). An additional purpose was to collect ASIRAS Ku-band radar data over an interior Antarctic region around 88°S, 135°E, in order to provide data to investigate anomalous patterns seen in CryoSat ice sheet elevation changes. Given the costly and complex logistic operations in the interior of Antarctica, a whole suite of airborne geophysics instruments were flown, providing geophysical and glaciological exploratory science data in virtually unknown regions of Antarctica. The data types collected consisted of:

- *Gravity data (with Lacoste & Romberg and iMAR IMU gravity sensors)*
- *Lidar data (swath high-resolution laser scanning of snow surface)*
- *Magnetic total field data*
- *Ice penetrating 150 MHz radar data (giving ice thickness data)*

And for a single flight from South Pole station

- *ASIRAS Ku-band coherent radar data (CryoSat proxy)*

All flights were done with supporting precision GPS and IMU (Inertial Measurement Unit) data for aircraft positioning and attitude determination. Ground reference stations for GPS and magnetic measurements were operated as well, and gravity reference points for the survey established by links to the absolute gravity site at McMurdo base, and the reference gravity point at Rothera Research Station on the Antarctic Peninsula.

The logistics conditions in the interior of Antarctica were truly challenging, with the initial part of the airborne operations carried out from two remote field camps – FD83 in deep interior East Antarctica, established in cooperation with NPI – and the Thiel Mountains camp in the Transantarctic Mountains region, established in cooperation with BAS. Aviation fuel at these sites was provided by commercial operators (ALCI air drop or ALE tractor trains). A total of 38 survey flights were carried out, with details listed in Appendix 1 and [RD1], and shown in Fig 1. The survey flight pattern focussed on un-surveyed regions of the "grid-north" part of the polar gap, with some "grid south" regions filled in and rectified by older campaign data and two new gravity-only lines acquired by US partner LDEO as part of the ROSETTA project.

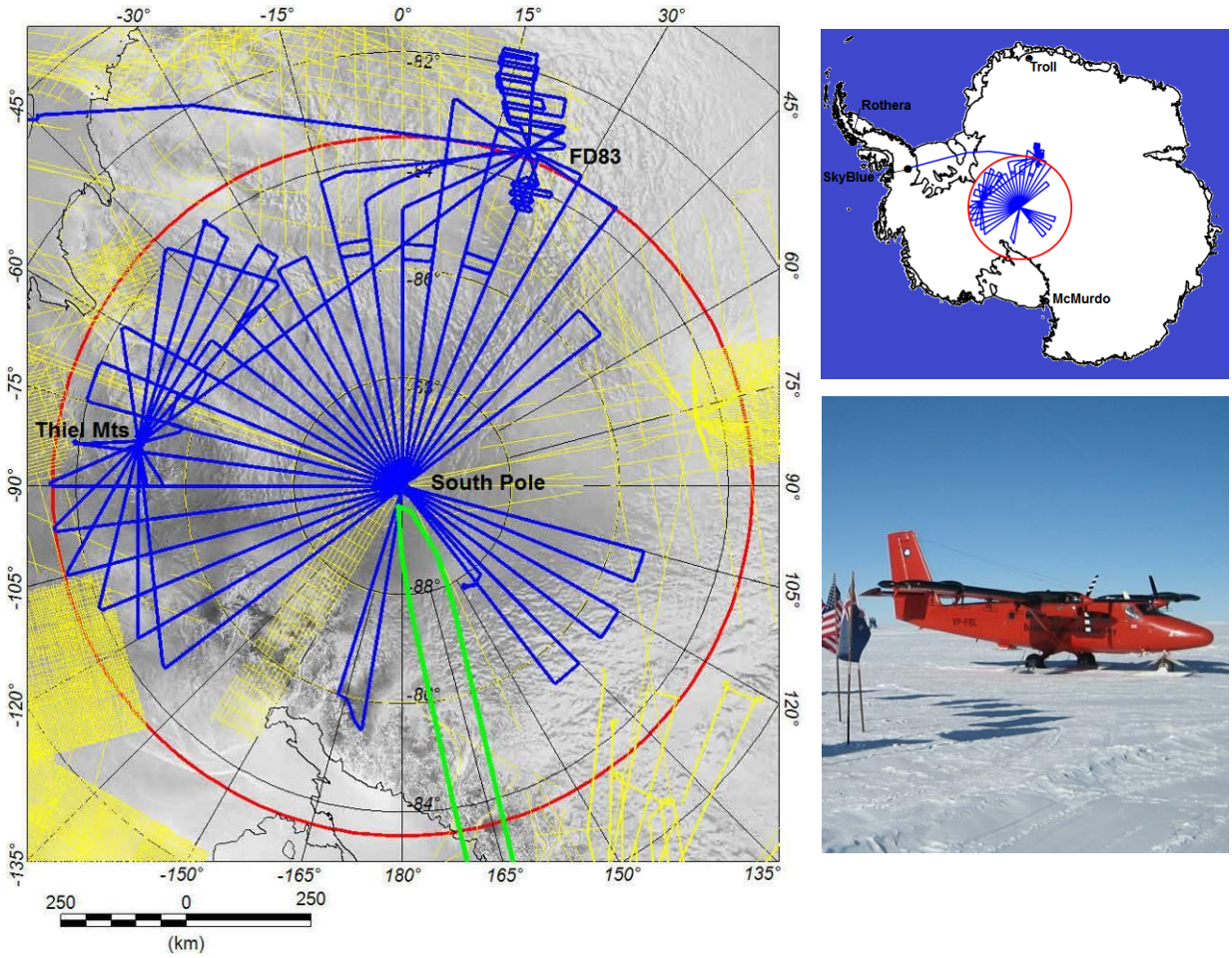

Fig.1. PolarGap gravity flight tracks of central Antarctica (blue), as flown with BAS Twin-Otter aircraft . The yellow lines show existing older gravity data, and green radial lines profiles flown by Columbia University.

2. AIRBORNE SURVEY INSTRUMENTS AND NAVIGATION PROCESSING

The survey instruments were installed in the BAS Twin-Otter as outlined in Fig. 2 and Fig. 3. The installation took place in the hangar at the British Rothera Base, except for ASIRAS, which was installed outdoors at South Pole (-30°C), after uninstalling the gravimeter and the ice penetrating radar due to weight limitations.

Gravity was measured with a ZLS-modified Lacoste and Romberg (LCR) gravimeter S-83, belonging to BAS. The LCR gravimeters have very low and stable drift, and are a well proven aerogravity system. We additionally flew a high-end inertial survey system (iMAR RQH-1003, provided by TU Darmstadt), which has been proven to give high resolution gravity at the mGal level in recent DTU-Space surveys in Chile and Malaysia. The combination of LCR and IMU gravity combine a long-term stability and a short term dynamic linearity and thus are capable of producing broad-band high-accuracy measurements. An additional lower-grade BAS IMU (iMAR FSAS), flown primarily to provide back-up roll and pitch for the laser scanner, turned out also to be a potential useful aid in gravity processing.

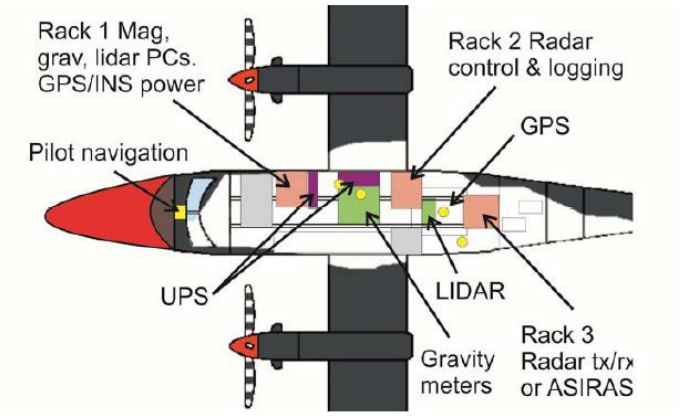

Fig. 2. Installation of instruments in Twin Otter. IMU's located on floor forward of gravimeter

Fig. 3. Left: Forward look in of the cabin, with LCR gravimeter sensor and magnetometer and power conditioner rack unit; right: ASIRAS installation in the back of aircraft cabin.

The Total Magnetic Field intensity (TMI) was measured with two wingtip-mounted Scintrex CS-3 Cesium vapour magnetometers. Proton procession magnetometers from DTU and BAS were used for monitoring and correcting the aeromagnetic data for diurnal variations and were installed at FD83 and Thiel Mountains. A US fluxgate reference magnetometer at South Pole was used as well.

Ice penetrating radar measurements were carried out using the BAS 150 MHz in house developed radar system. The system uses under-wing mounted dipole antennas, and yielded reliable ice thickness measurements in most areas, except in the deepest parts of subglacial basins. An uncontrolled shutdown of the radar system at the end of flight P22 resulted in damage to all connected amplifiers in the radar receiver. This problem was repaired in the field using spare amplifier channels, and the radar system performance for flight P24 and subsequent missions appeared as before in the in-flight QC monitor.

Lidar ice sheet elevation data were measured with a Riegl Q240i laser scanner (same type as used in the ESA CryoVEx campaigns). These data have an accuracy of a few cm, due primarily to the resolution of kinematic GPS positioning, typically at the 10 cm rms level. To estimate angular

offsets of the laser scanner data, calibration flights were made over runway at Rothera, as well over GPS-surveyed buildings at Rothera and South Pole station.

Precise GPS processing for positions and attitude were provided by multiple onboard and reference geodetic GPS systems (Javad, Novatel, and Leica GPS receivers). The *WayPoint* software was used for several GNSS position solutions using IGS precise orbits and reference GPS stations at the aircraft bases and using the permanent GPS stations at Rothera and South Pole station. A "best" solution was merged with roll, pitch and heading from an onboard iMAR RQH-1003 unit, processed using an 18-state custom designed Kalman filter for estimation of position, attitude and gravity components. The implementation and processing using the Kalman filter software was done by David Becker, Technical University of Darmstadt, Germany, as part of the subcontract to DTU Space for rental of the RQH-1003.

Fig. 4. South Pole Station GPS reference (right antenna). The roof used to calibrate lidar and ASIRAS.

3. AIRBORNE GRAVITY PROCESSING

The raw airborne gravity measurements from the airborne LCR gravimeter S-83 was processed by Arne Olesen, DTU-Space, based on the Waypoint GPS positioning solutions. The processing, in addition to the stand-alone LCR processing, also consists of merging with IMU gravity Kalman filter independent gravity estimates, using an in-house developed draping approach. This ensured that the long-wavelength, bias-stable LCR data are optimally merged with the more linear, but drifting, results of the RQH-IMU; for details see [RD2] and [RD3], and for a line processing example Fig. 5.

The processing parameters for the LCR gravity data included a 130-150 sec long 2nd order Butterworth along-track filtering, corresponding to a ca. 6 km half-width spatial resolution. The flight elevations were generally low level (1200 ft AGL), due to limited range of the Riegl lidar, but occasionally higher due to fog or low-level clouds; flight altitudes varied between 2.9 and 4.3 km. Fig. 6 shows the final processed gravity disturbance.

The overall accuracy of the airborne gravity processing was 2.2 mGal r.m.s., as inferred from 129 cross- over points, not taking into account the difference in heights at the cross-over points. This is a highly satisfactory result, given the rough operational conditions (field camps, temperatures

down to -30°C), and the fact that the BAS Twin-Otter did not have an autopilot, which is usually a requirement for high-quality, bias-free aerogravity. It should be pointed out that *no* cross-over adjustment was performed on the data, so the data level of every single line is determined only by the gravimeter "apron" values, i.e. the stationary readings before or after flights.

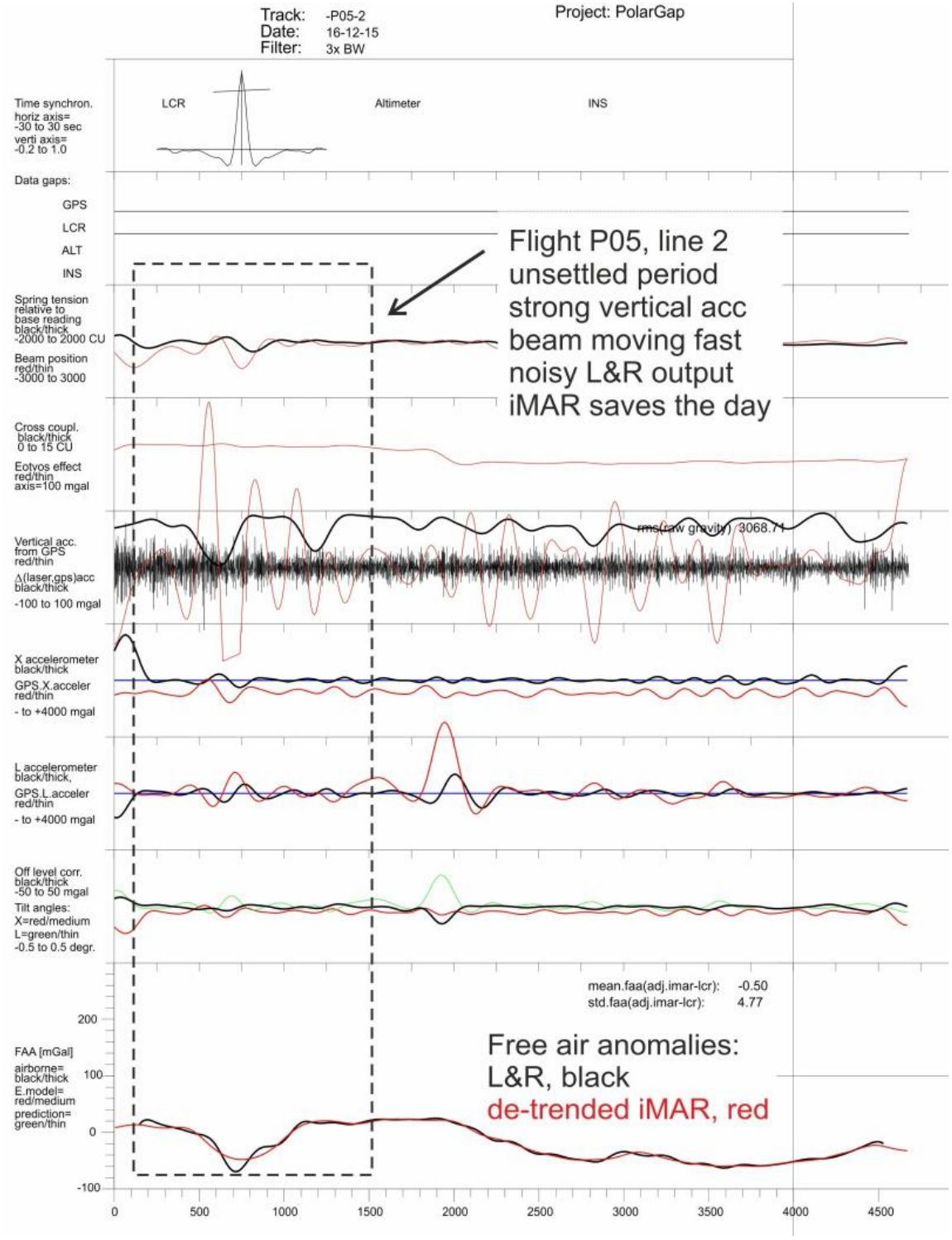

Fig. 5. Example of processing graphics used to evaluate results on a line-by-line basis. The shown line P05 highlights the importance of the "hybrid" LCR-iMAR processing through a period of turbulence.

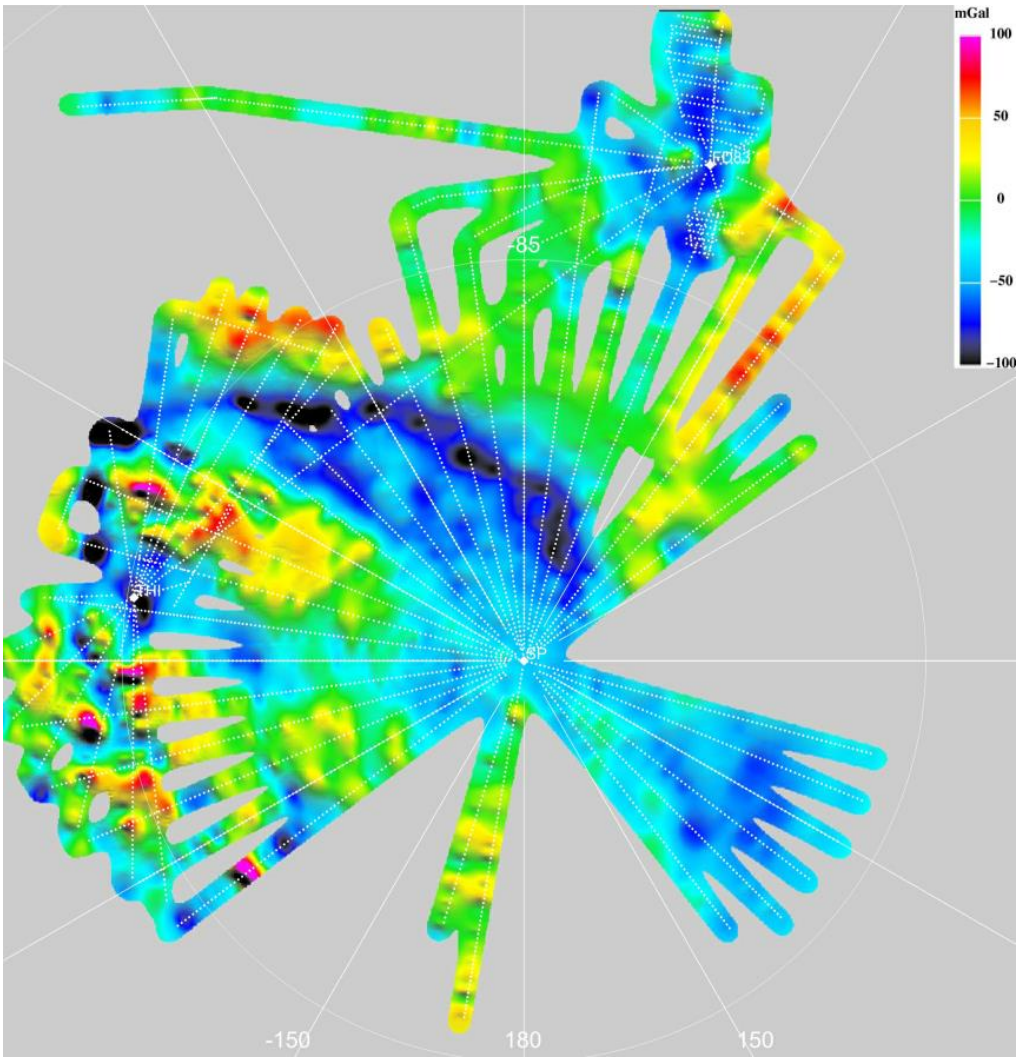

Fig. 6. Final gravity disturbances (i.e. gravity anomaly using ellipsoidal heights) from the PolarGap survey. The gravity anomalies confirm the existence of a very deep subglacial valley ("Pensacola-Pole basin").

The airborne survey was based on a reference gravity network established and linked to absolute gravity ties in McMurdo and at Novo, as well as to IGSN-71 gravity reference points in South America. Accurate absolute gravity values at the aircraft parking spots are essential for consistency with GOCE satellite, and typically not something that is not as high priority for geophysical-oriented surveys.

The gravity ties were done with LCR land gravimeters G-784 (BAS) and G-867 (DTU), linked to earlier surveys and reference stations at McMurdo and Rothera, and adjusted in a least-squares process, keeping earlier network gravity points from the ICEGRAV 2010-13 adjustment [RD4] fixed. Complications arose from the fact that South Pole station is actually on moving ice, with elevations lowering by approximately 19 cm/yr, as inferred from the permanent GPS on the station; this will increase the base gravity values by about 0.05 mGal/year. Taking this apparent temporal gravity change into account, the South Pole reference gravity fits to within 0.2 mGal of earlier measurements in the period 2008-13; for details see [RD1]. The PolarGap reference survey network is shown in Fig. 7, and the used PolarGap gravity reference values shown in Table 1.

Table 1. *Absolute gravity values used for the PolarGap survey*

Rothera, hangar	982468.05 ±0.1
McMurdo, absolute gravity hut	982970.543 ±0.01
FD83 aircraft parking 2015/16	982272.43 ±0.2
Thiel Mountains camp	982691.25 ±0.2
South Pole, reference point in utility tunnel	982316.47 ±0.1
South Pole, Twin-Otter parking spot	982313.63 ±0.1
South Pole, main apron at fuel tanks	982313.06 ±0.1

It should be noted that the reference Rothera g-value was based on multiple gravimeter ties to Punta Arenas and Ushuaia in the period 2010-13; the older BAS reference gravity value, based on several 1999 ties, was 0.6 mGal lower. The South American ties were therefore deemed less reliable. A later absolute re-observation of the primary Ushuaia reference point PF1N(383) by IGN, Argentina, gave a value of g = 981468.935 mGal (A. Zakrajsek/D. Pinon, pers.comm.). This confirmed the used ICEGRAV value to be correct within 0.07 mGal, and thus confirming the overall absolute level of the PolarGap survey to be correct.

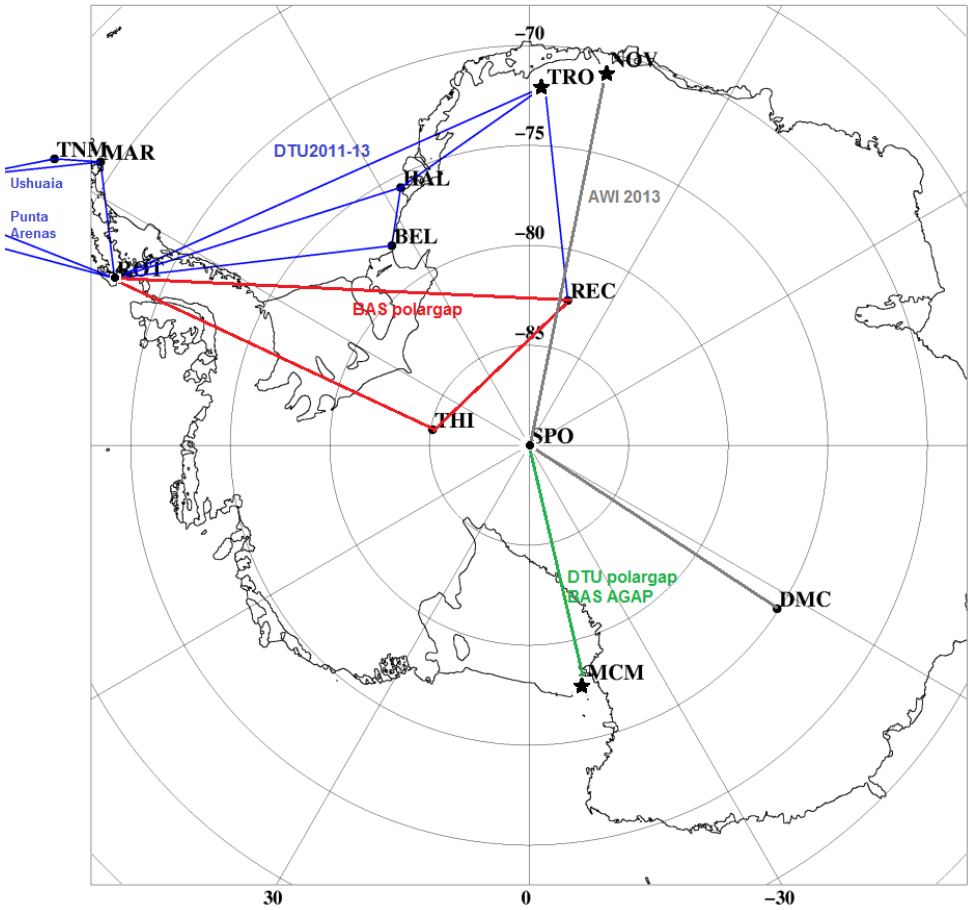

Fig. 7. Gravity network in Antarctica supporting the PolarGap airborne gravity survey (red and green). Additional gravity ties include data from the ESA 2013 Dome-C airborne gravity campaign (grey, ties processed by DTU Space), and ties from ICEGRAV (blue). Stars indicate absolute gravity points.

4. COMPARISON TO EXISTING GRAVITY DATA AND PREDICTION OF GRAVITY GRADIENTS

A number of existing airborne gravity surveys cover parts of the polar gap region. Some of these data are recent, and with good control of absolute gravity accuracy (e.g. NASA IceBridge data), while other data sources are from a number of geophysical surveys extending back to the early 1990's of earlier, with larger errors, and – for some surveys – no absolute reference. Furthermore some data sources are given only as (lat, lon, free-air anomaly) files, without any further description, e.g. in terms of reference values, flight heights and type of anomalies used. However, high-quality recent data sets such as NASA IceBridge and the DTU ICEGRAV surveys [RD7], together with PolarGap data, allows transformation of older data to a consistent system. The older data are therefore useful to augment the PolarGap data in missing data regions.

The data used in the sequel are assumed to represent *gravity disturbances* δg, i.e. gravity anomalies computed from ellipsoidal heights of the aircraft; such anomalies are in a geophysical context often referred to as free-air anomalies Δg; this is inconsistent with the geodetic definition, which assumes heights above the geoid. The difference between the two definitions of Δg is often large (10-20 mGal), and care has been taken to consistent data preparation.

Fig. 8 (right) shows the major airborne gravity data sets used for cross-over comparisons, relative to a "reference" data set consisting of ICEGRAV, PolarGap and IceBridge data. The older data sets have entered into the recent Antarctica Gravity Grid compilation by Scheinert et al. [RD-5], and references to many of these surveys can be found therein. In addition AWI and DTU Space cooperated to reprocess some recent data (especially the AWI RECISL 2013 data) to fill in important data voids, and two radial lines from the ongoing US Rosetta project, supplementing the PolarGap survey, were provided by LDEO/Columbia University.

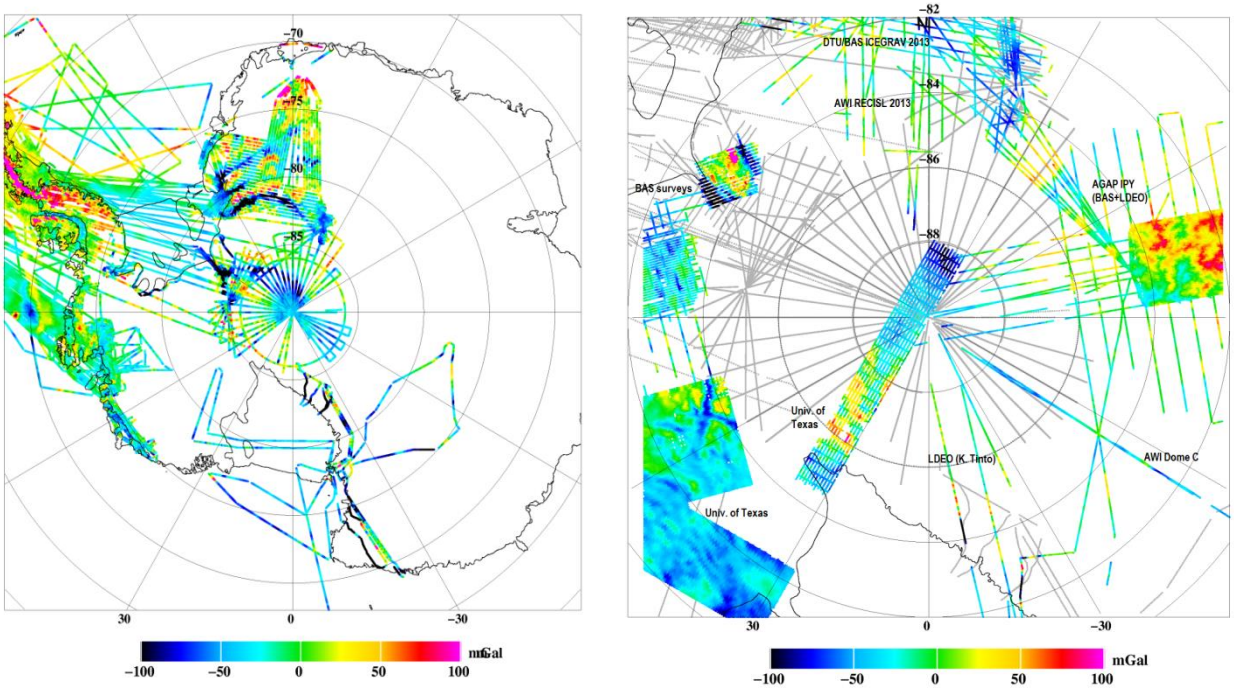

Fig. 8. Gravity disturbance data sets, used for internal cross-over evaluation. Left: The "reference" IceBridge, IceGrav and PolarGap data; right the major airborne fill-in data sets within the extended polar gap south of 82 ° (reference lines shown in grey). Older surface gravity over the Ross ice shelf not shown.

The comparison between the different data sets has been done using a collocation prediction approach, where nearest data points within a search radius of 0.5-4 km distance are used to predict one data set from another data set (different search radii are needed due to different data spacings). Comparisons between the different data sets are shown in Table 2. It should be noted that no upward/downward continuation was done on these data sets, to take into account differences in flight elevations; this therefore gives rise to large comparison errors in some cases where flight elevations differ significantly. Overall, though, most data sets show a reasonable fit, with IceBridge, PolarGap and BAS data fitting well (when flight altitudes are close), while the older University of Texas data were clearly off in terms of absolute gravity levels, and these data have therefore corrected by the estimated biases shown in Table 2.

Table 2. *Comparison of different gravity data sets (δg-$\delta g_{PolarGap}$ in the extended polar gap). Unit: mGal*

Survey	Assumed error	Search radius	x-over zone pts	Mean	Stddev
AGAP 2008-9 (BAS / LDEO, atm. corr. applied)	3.0	.5 km	413	-0.8	9.7
IceGrav 2009-13 compared to PolarGap	2.0	.5 km	341	0.9	3.3
IceBridge 2009-14 (4km) compared to PolarGap	1.0	4 km	327	-3.1	9.5
IceBridge 2009-14 (2 km), h < 5 km	1.0	2 km	175	-2.3	3.7
IceBridge 2009-14, h < 5 km, lat < 87 S	1.0	2 km	24	-0.1	2.9
AWI Dome-C transit (DTU processed)	5.0	1 km	93	(-0.2)	(2.7)
AWI RECISL (DTU processed)	5.0	1 km	329	(0.1)	(0.9)
LDEO Rosetta (OIB x-overs), all heights	4.0	4 km	120	31.3	29.7
LDEO Rosetta (OIB, 86 S circle only)	4.0	4 km	6	2.3	1.0
Older BAS data	4.0	2 km	459	-0.5	6.8
Univ. Texas grid data, PolarGap+OIB comparison	5.0	1 km	616	39.0*	7.3
Univ. Texas grid data (South Pole Transect)	5.0	4 km	29.6	29.6*	5.0

All of the above data set were merged into one large data set for the Polar Gap region, shown in Fig. 9. It is seen that the combination of the older data, IceBridge, and the new PolarGap and LDEO/AWI data, give a nearly complete overage of the polar gap, at least at GOCE resolution.

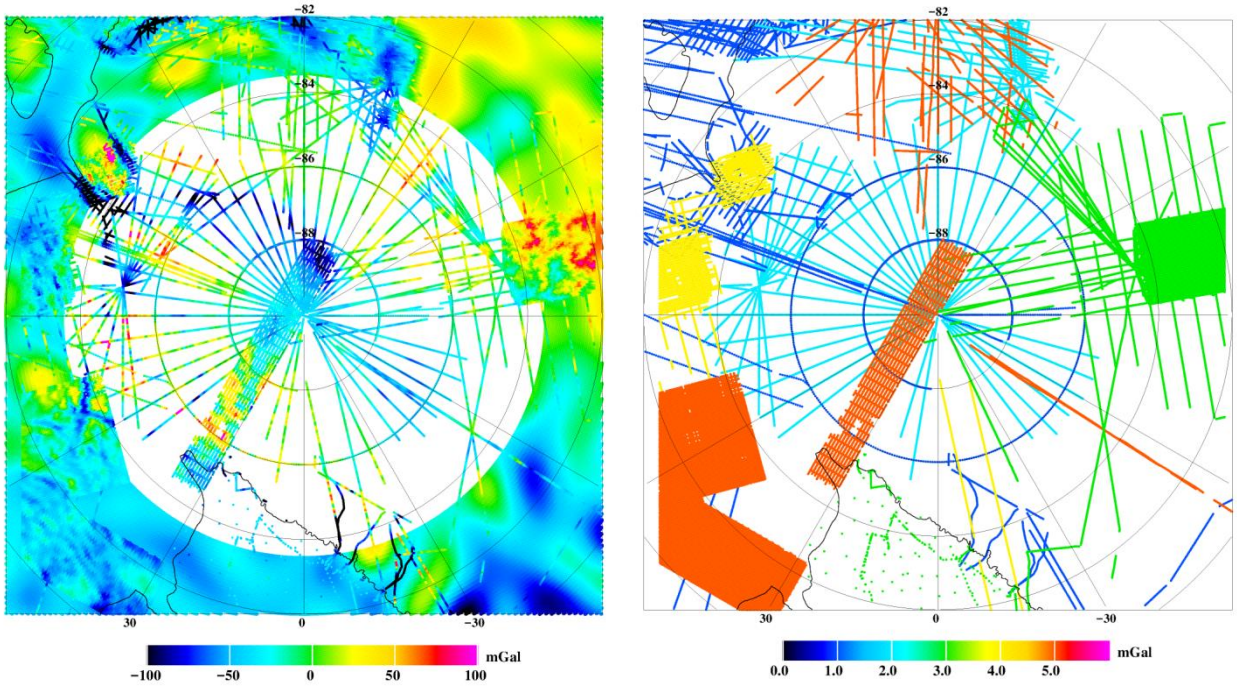

Fig. 9. Merged gravity data set. Left: δg from airborne data and GOCE; right: assigned standard deviation.

The combined surface and airborne gravity data set shown in Fig. 9 have been thinned to 10 km resolution (in the SCAR polar stereographic projection, reference parallel at 71°S), in order to perform a least squares collocation prediction of ***gravity gradients*** (and gravity anomalies) at altitude. The least squares collocation process is a standard geodetic method to model different gravity field quantities (gravity, geoid or gradients), based on a modelled covariance function. The method is based on a solution of a large set of linear equations, hence the need for the (slight) thinning of data, and limiting the data used to an extended polar gap south of 82.5°S, in order to keep the number of linear equations manageable. The collocation equations are of form

$$s = C_{sx}(C_{xx} + D_{xx})^{-1} x$$
$$x = \{\Delta g_1, \Delta g_2 ...\} set\ of\ known\ data\ pts$$
$$s\ \ is\ a\ prediction\ \ pt$$

with estimated standard deviation of the predictions given by

$$\sigma^2{}_{ss} = C_0 - C_{sx}{}^T (C_{xx} + D_{xx})^{-1} C_{sx}$$

Here C are the covariance/cross-covariance matrices, and D the assumed input data errors. The covariance functions used here are of the Tscherning-Rapp type, and computations carried out in the GRAVSOFT suite of programs [RD-6]. The best-fitting covariance function is shown in Fig. 10.

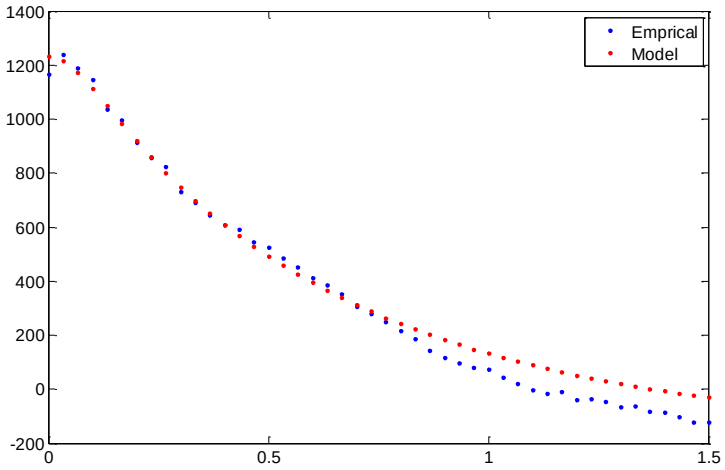

Fig. 10. Covariance functions used for the gravity covarience functions. Units in degrees (x-axis) and mgal^2 (y-axis). A reference field to spherical harmonic degree 60 (GOCE RL5 "direct") has been subtracted prior to computations.

Examples of the gravity gradients computed at GOCE altitudes, along with the estimated errors, are shown in Fig. 11 and 12. Gravity gradient grids were computed at altitudes 225 km and 255 km, to allow interpolation to actual GOCE flight altitudes. It should be noted that the GRAVSOFT convention for gravity gradients differ from the ESA GOCE conventions as outlined below in Table 3. Generally the usual local cartesian system for gravity gradients in an (N, E, Up) coordinate system are not well-suited for representing polar gravity gradients; instead a local (N_{grid}, E_{grid}, Up) in polar stereographic projection might be preferable for graphical displays and avoidance of the south pole singularity. However, for ease of global use, the final PolarGap gradients have been provided in the conventional lat-lon-height system.

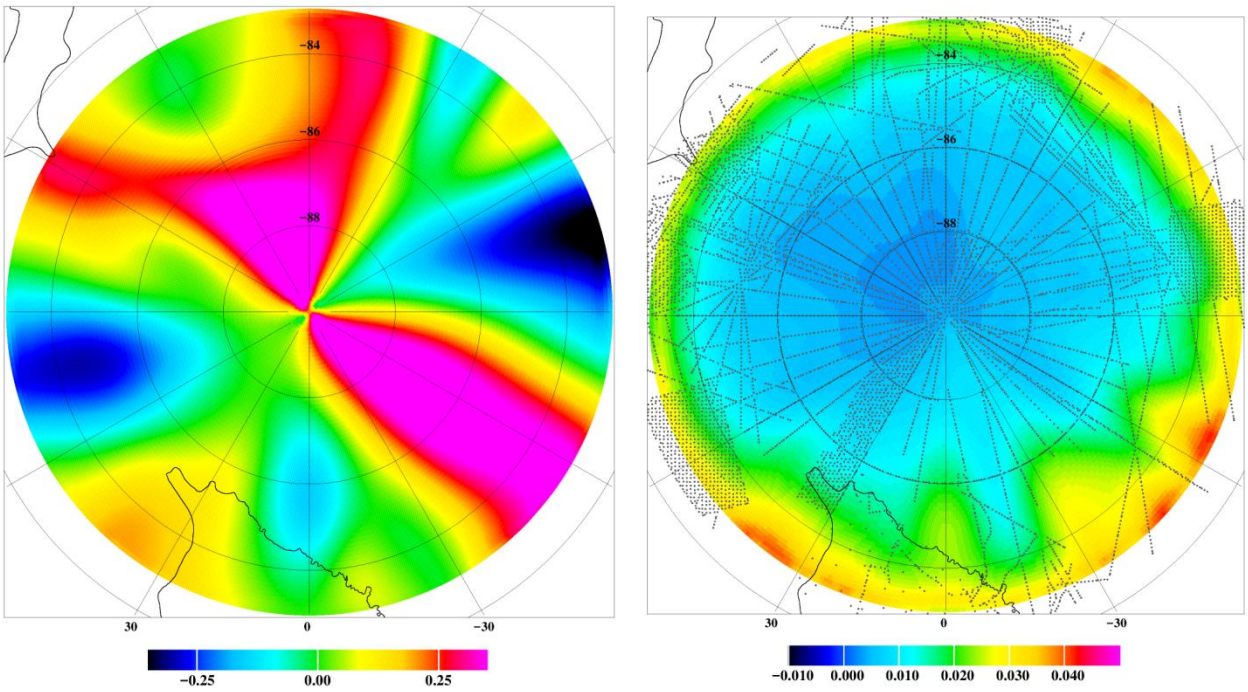

Fig. 11. Left: Example of predicted gravity gradients (T_{xx}); right: estimated error of T_{zz}. Units: Eotvos.

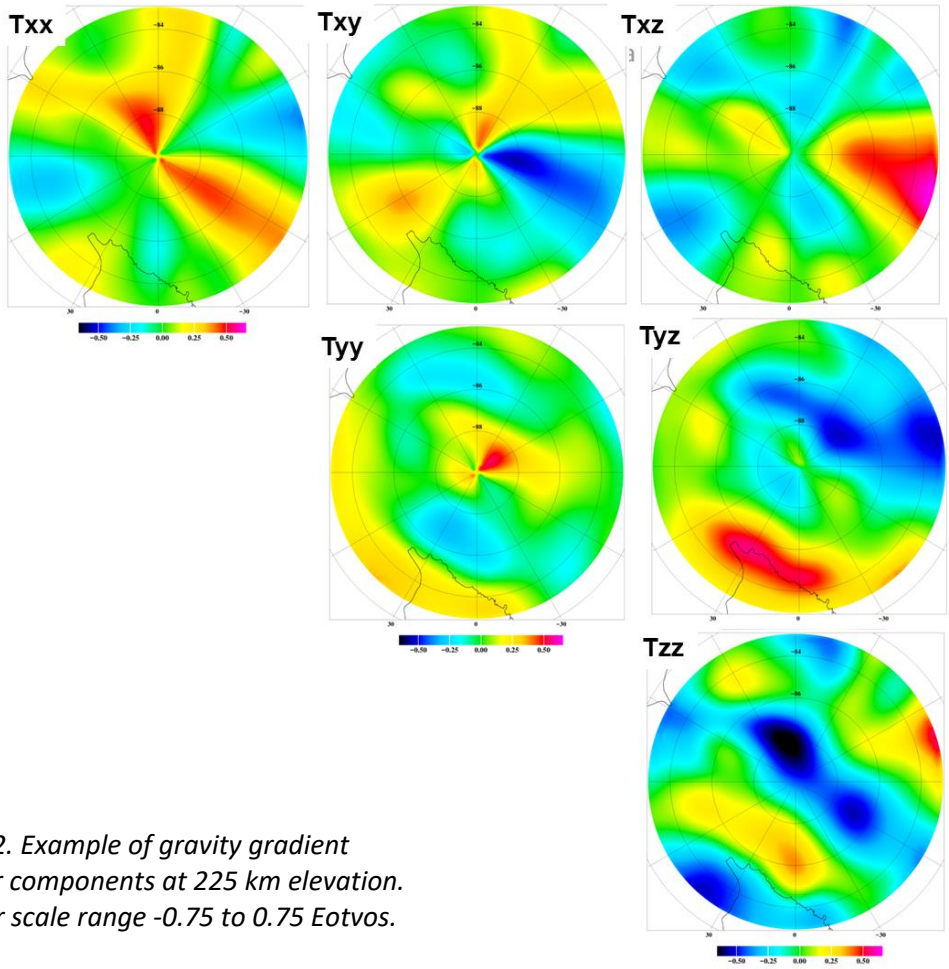

Fig. 12. Example of gravity gradient tensor components at 225 km elevation. Colour scale range -0.75 to 0.75 Eotvos.

Table 3. *Relationship between the ESA GOCE LNOF system (N-W-Up) and the GRAVSOFT (E-N-Up) gradient coordinate systems (H. Yildiz)*

ESA GOCE	GRAVSOFT
$T^{LNOF}zz$ =	$T^{G}zz$
$T^{LNOF}xx$ =	$T^{G}yy$
$T^{LNOF}yy$ =	$T^{G}xx$
$T^{LNOF}xy$ =	$-T^{G}xy$
$T^{LNOF}xz$ =	$-T^{G}yz$
$T^{LNOF}yz$ =	$T^{G}xz$

For a comparison of the GOCE gradient observations and the upward continued gravity gradients, fig. 13 shows composite plots of the upward continued gravity gradient predictions, and the actual GOCE gradient observations north of 82.5°S (based on the ESA GOCE RL5 "direct" spherical harmonic expansion), in the NEU coordinate system. It is seen that overall a good consistent agreement across the GOCE orbit limit at 83.5°S is obtained.

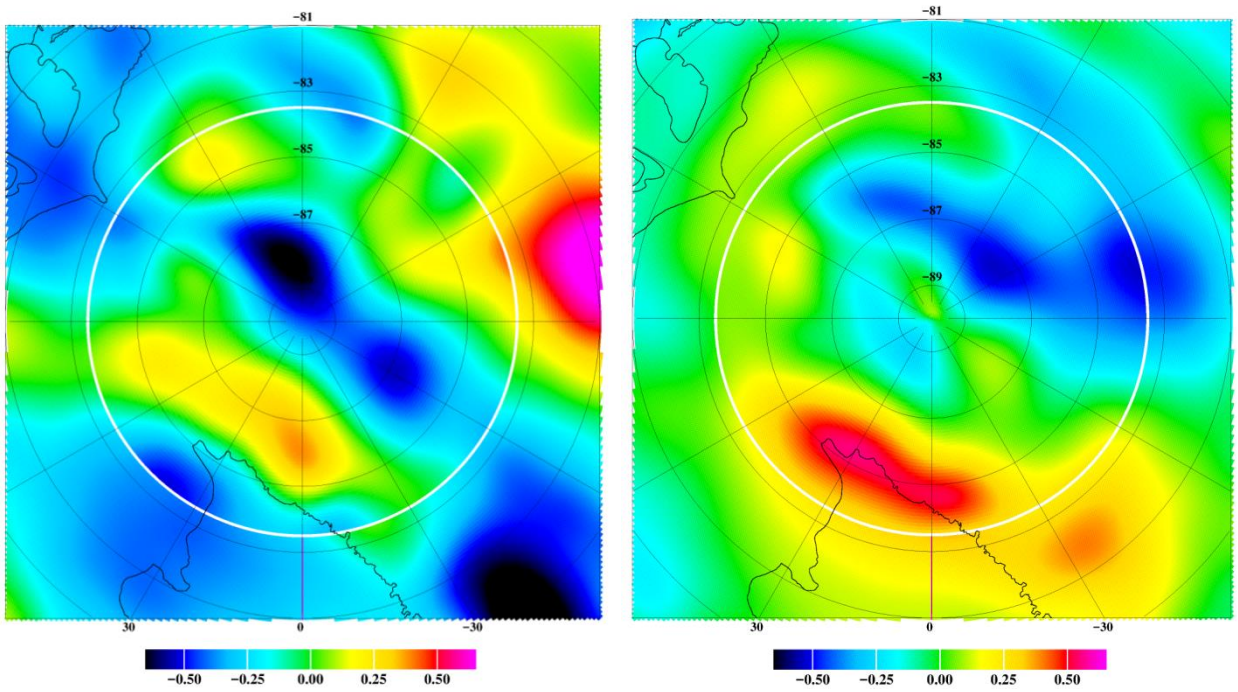

Fig. 13. Example of predicted gravity gradients from available gravity data south of 82.5°S, and the corresponding GOCE observations, at altitude 225 km. Left: T_{zz}, right: T_{yz} component (NEU). Units: Eotvos.

5. LIDAR DATA PROCESSING

An example of lidar data over the Amundsen-Scott South Pole base area is shown in Fig 14, based on GPS solutions and aircraft attitude from the lower grade iMAR FSAS IMU (errors in roll and pitch can be seen as some weak striping across the scans), without proper calibration of offset angles. The flights over the South Pole area was done on two days (P26 and P36), at different flight elevations above ground level (ca. 400 m and ca. 600 m). Laser scanning over the pole itself presented challenges related to software singularity bugs, and a few anomalies right at pole can still be seen. Otherwise there is a good agreement between the four different scans, and many surface features can be seen, including the main station building and cargo lines.

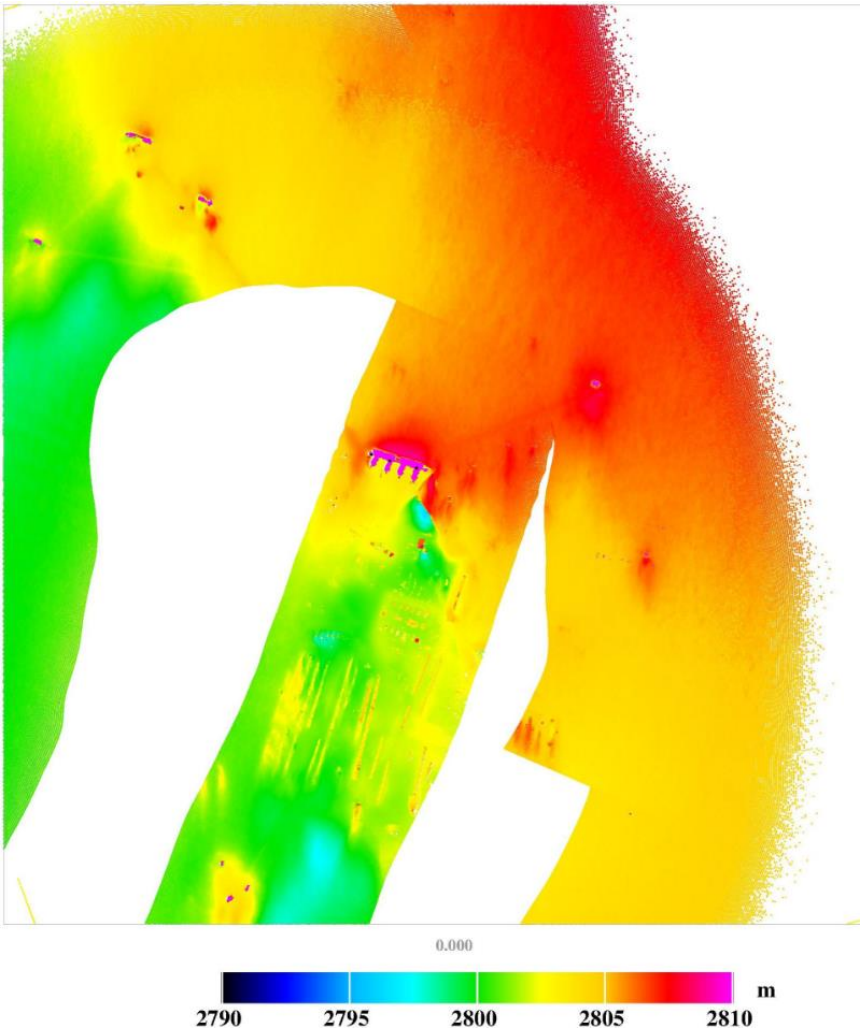

Fig 14. Lidar profiles over the South Pole base area. The main building complex, the Amundsen-Scott South Pole Station, is seen as a purple structure in the middle of the plot. Three stationary GPS observations at building roof corners, shown as black dots, showed a 5 cm agreement with the airborne lidar heights, and confirmed the lidar calibration from Rothera station and Recovery Lakes.

It is evident from Fig. 14 that the Riegl Q240i lidar works well around 400 m AGL, but loose some signal at 600 m; most flights were flown at 400 m AGL or lower, but due to the need for constant elevation flights for gravity, there will be a large range of elevations in the lidar data. Only for the ASIRAS flight a constant elevation (AGL) of ca. 450 m was maintained throughout the flight. The final processing of lidar data was done with the DTU in-house program QSCAN, update to handle the South Pole singularity. The software combines precise differential positions from GPS with attitude information from the INS and range measurements from the lidar system, to form point clouds at ~1 m resolution, referred to the WGS84 ellipsoid.

A critical step in the processing is the estimation of installation biases between the inertial system and the lidar (also known as boresight alignment). A building with known corner coordinates (the Bonner Laboratory at the Rothera Research Station), was overflown 4 times with 90 degrees azimuth offset during the initial test flight. Installation biases from these passes were estimated to be -0.10^{o} for pitch, -0.50^{o} for roll and -0.50^{o} for heading. The Bonner Laboratory test flight data is shown in Fig 15, along with results from Rothera runway overflights. The runway was surveyed with a vehicle equipped with GPS, and the difference

between the ground based survey and the airborne data is shown as colored dots, with airborne data interpolated to the dense ground truth data points. Two such passes were done and gave similar results. The mean difference was 4.5 cm with a standard deviation of 6.0 cm. The mean difference could be considered a system bias, whereas the standard deviation at least to some extent should be ascribed to interpolation errors, as the runway surface is rather uneven.

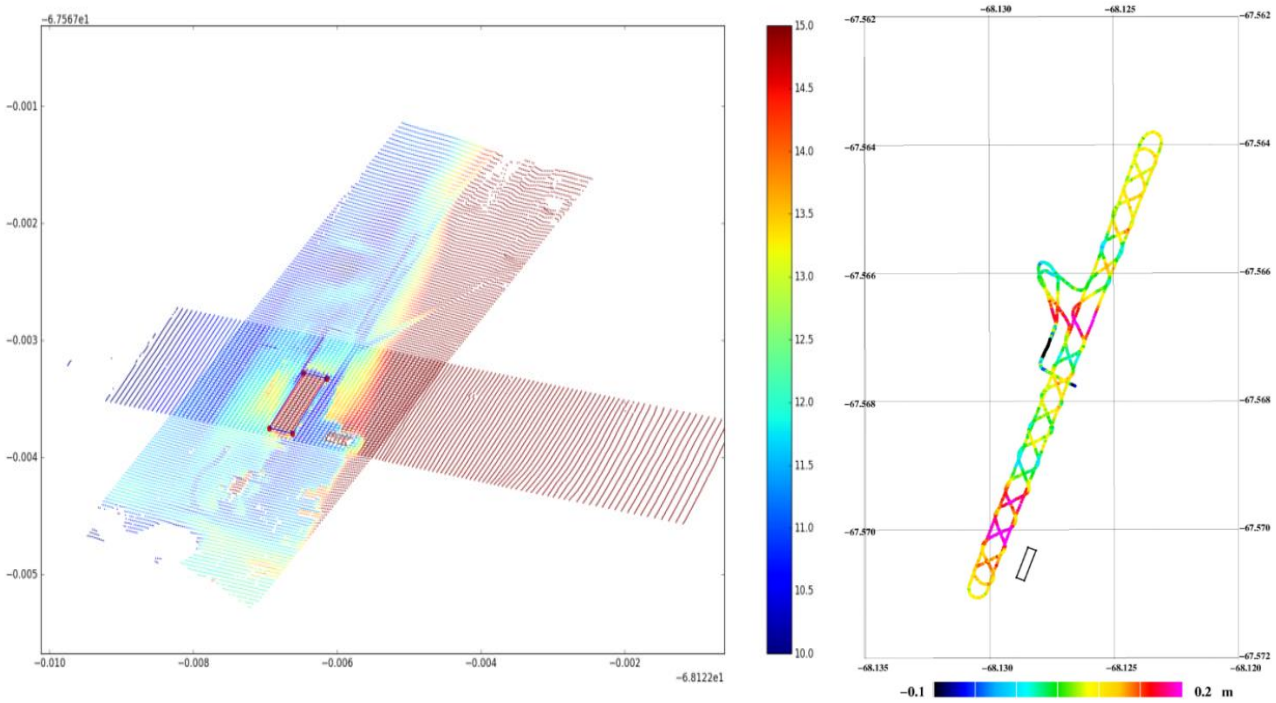

Fig 15. Left: Bonner Laboratory overflights for installation bias estimation at Rothera. Right: difference between airborne lidar and ground vehicle GPS results over the runway, including the hangar apron. The box to the lower right of the runway is the outline of the Bonner Laboratory.

Survey flights over the subglacial Recovery Lakes in East Antarctica gave an opportunity to fine-tune the roll bias estimate. The Recovery Lakes snow surface are very flat features, and are perfectly suited for this purpose as lidar results in this case are almost independent of errors in pitch and heading. Analysis of data from two survey-line crosses showed an optimal estimate for the roll installation bias of -0.55°. The final installation bias estimate (boresight alignment) applied for all lidar processing was thus -0.10° for pitch, -0.55° for roll and -0.50° for heading.

Fig 16 shows the results from one of the survey line crossings over the Recovery Lake area. It is apparent that a small, residual systematic error is still present in the data. There is a perfect match in the centre of the swath, and to some extent along the diagonals, but systematic disagreement where centre values from one line is compared to edge values from the other line. The effect can be up to 20 cm along the edge of the swath, and likely due to internal hardware calibrations known to affect the Riegl units. It has not been possible to come up with a correction model that sufficiently reduces this effect. Potential users of the data are therefore advised to be careful to use data towards the outer edges of lidar swaths, due to the increased noise, especially for very precise surface height determination.

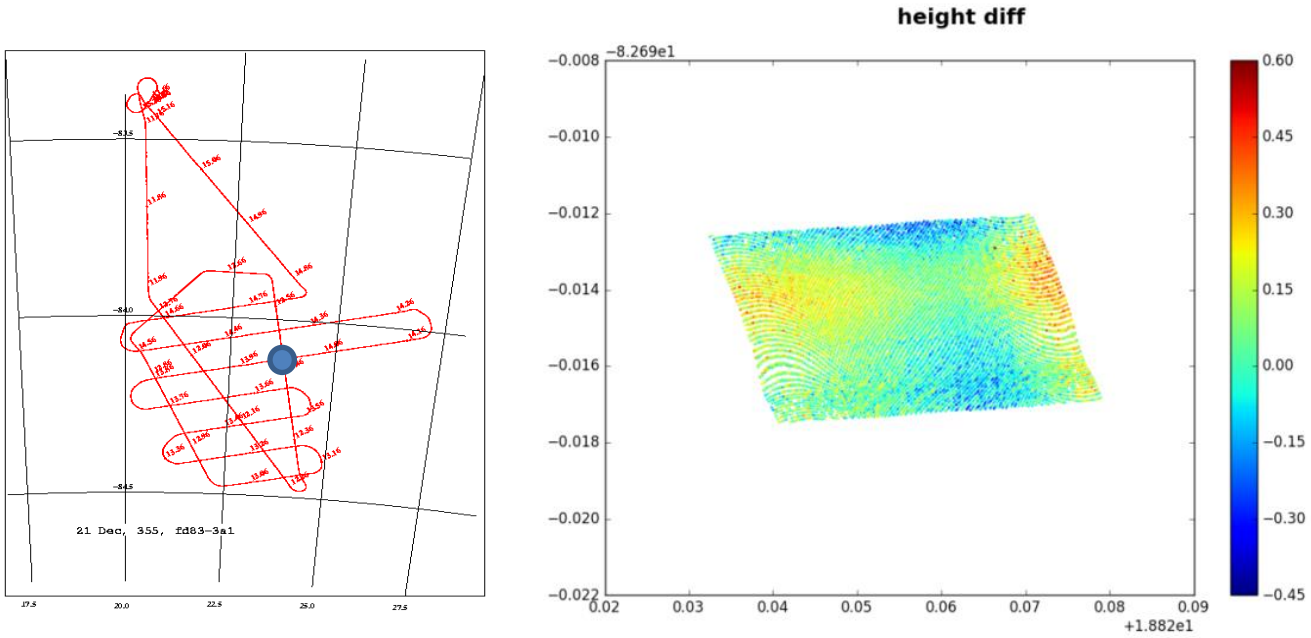

Fig 16. Example of analysis of a line crossing over the Recovery Lakes area, showing the systematic elevation differences at a lidar cross-over zone (blue dot). Left: the local flight ground tracks; right: difference between lidar heights of the crossing tracks.

The lidar results will also contain reflections from particles in the air, like snow crystals and occasional ground fog and wind-blown snow, so potential users of the data should apply some form of spike or threshold filter to remove none-terrain reflections. Near vertical results for the whole campaign after application of such a threshold filter is shown in Fig 17. These data are filling an important void in the DEMs of Antarctica; existing surface height models shows large errors beyond the coverage of IceSat and CryoSat.

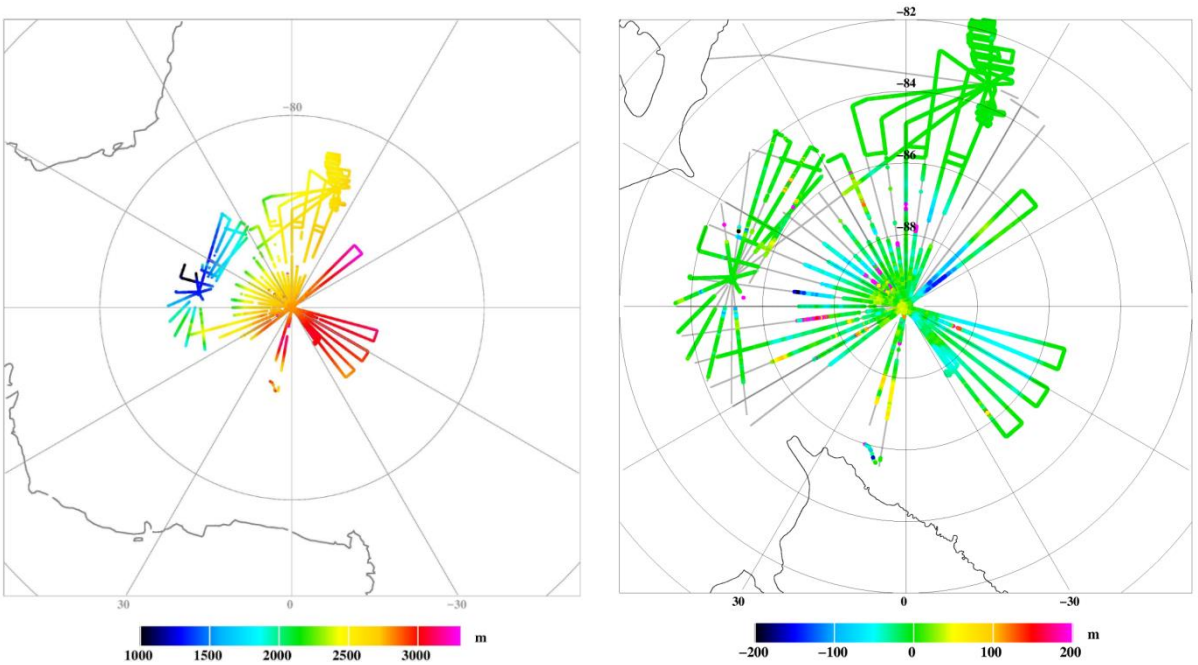

Fig 17. Left: near-vertical lidar results from the PolarGap campaign, after application of a threshold filter.Right: Difference between the PolarGap lidar results, and the IceSat-based BEDMAP2 DEM [RD11].

6. ASIRAS KU-BAND RADAR PROCESSING

The ESA ASIRAs Ku-band radar was flown in the PolarGap project only on one 4 hr flight – P37 – flying from South Pole Station to a region grid-SE of the South Pole at 87.8°S, cf. Appendix 1. The flight target was a localtion in a latitude band where earlier processing of CryoSat by MSSL has resulted in some strange "necklace" features in the elevation change signals.

Unfortunately logistics and weight constraints did not allow to fly ASIRAS along with the other geophysical measurements, and ASIRAS radar was therefore installed in the aircraft at the end of the PolarGap campaign at South Pole station, and the gravimeter unmounted. The central pattern flown at different headings around the East Antarctic 87.8°S, 146°E location is shown in Fig. 18.

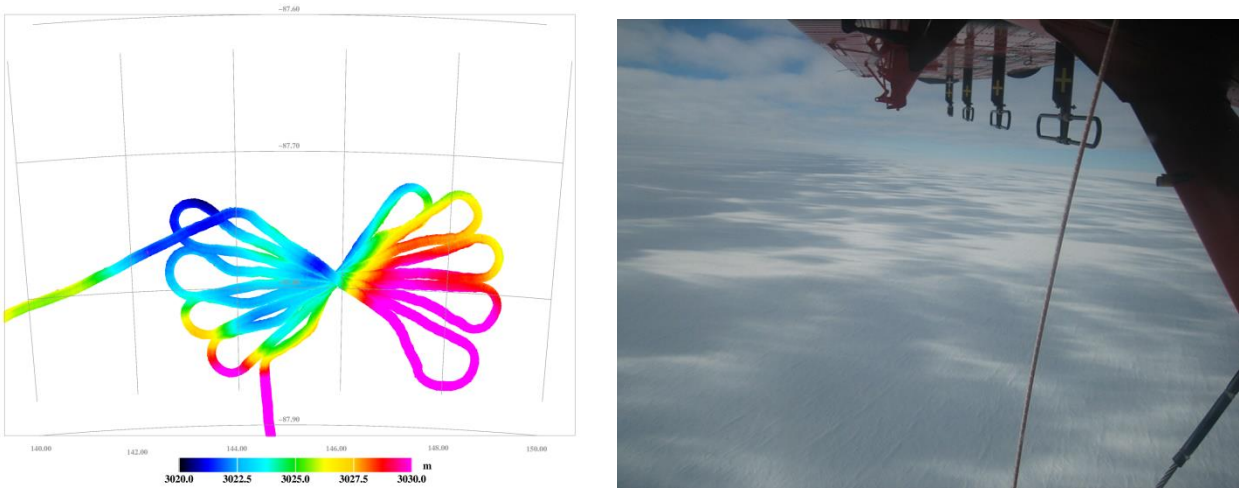

Fig. 18. Left: the ASIRAS flight pattern around 87.8°S, 146°E; colours show ellipsoidal heights from lidar. Right: the ASIRAS flight region, with surface sastrugi seen on the otherwise flat east Antarctic icesheet.

The ASIRAS was flown in low-altitude mode only, and a pass over South Pole station served as a calibration target. Veit Helm (AWI) processed the raw ASIRAS data into a L1B product, with some difficulty due to time tagging and out-of-range tracking problems. The ASIRAS L1B waveform data were subsequently retracked into elevations by an OCOG retracker, originally provided by Bob Hawley (Darthmouth College), and improved by Tim Jensen, DTU Space. Fig. 19 and Fig. 20 show some results of the retracking. Where the ASIRAS data are healthy, the difference in surface heights to lidar are around 6 m, mainly due to ASIRAS hardware range offsets (similar ASIRAS bias has been found in Arctic CryoVEx runway overflights). A more careful study of ASIRAS radar penetration effects relative to lidar is needed, but beyond the scope of this report.

For the overflights of South Pole station, it was possible to directly compare the ASIRAS retracked heights with the airborne lidar, and with the precise GPS measurements of the roof heights. This gave the heights shown in Table 4, confirming the ~5 cm r.m.s. estimated error of the airborne lidar central swath, and the ~6 m offset in ASIRAS OCOG heights.

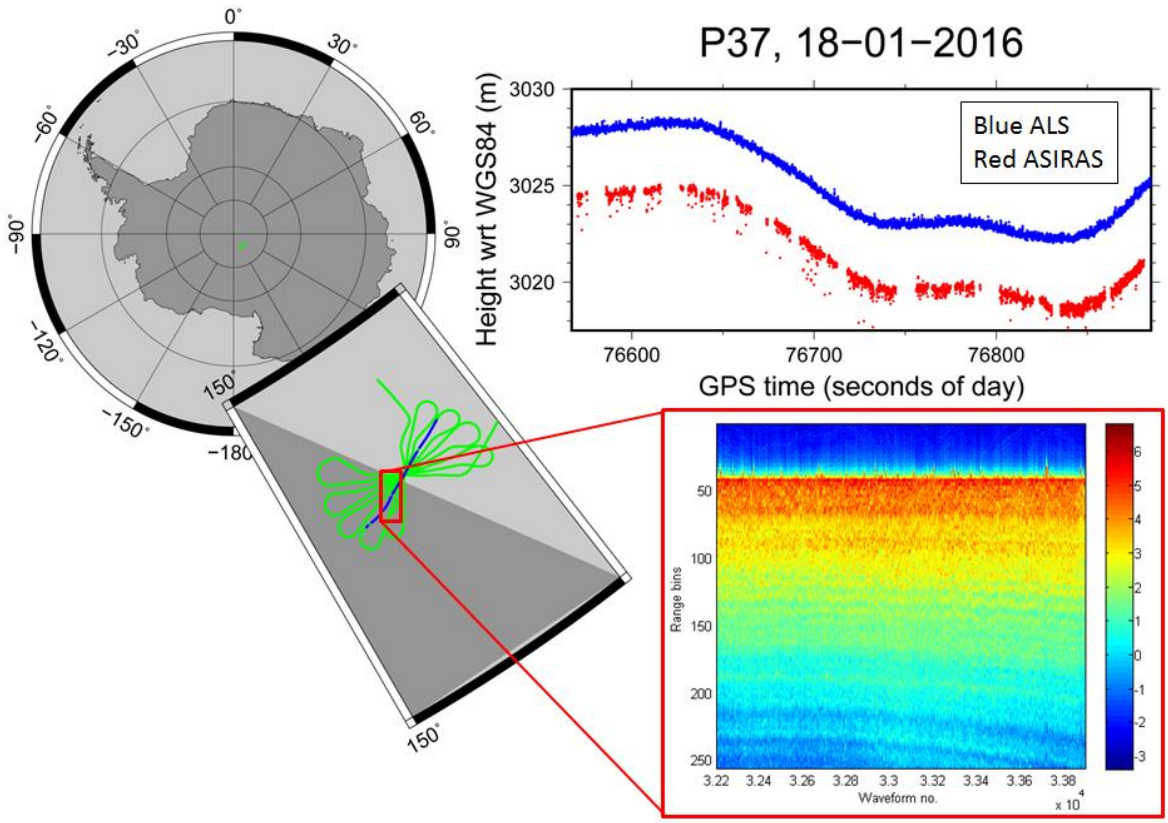

Fig. 19. Example of an ASIRAS L1B stack (colours represent normalized echo power), and a OCOG retracked surface along with lidar results.

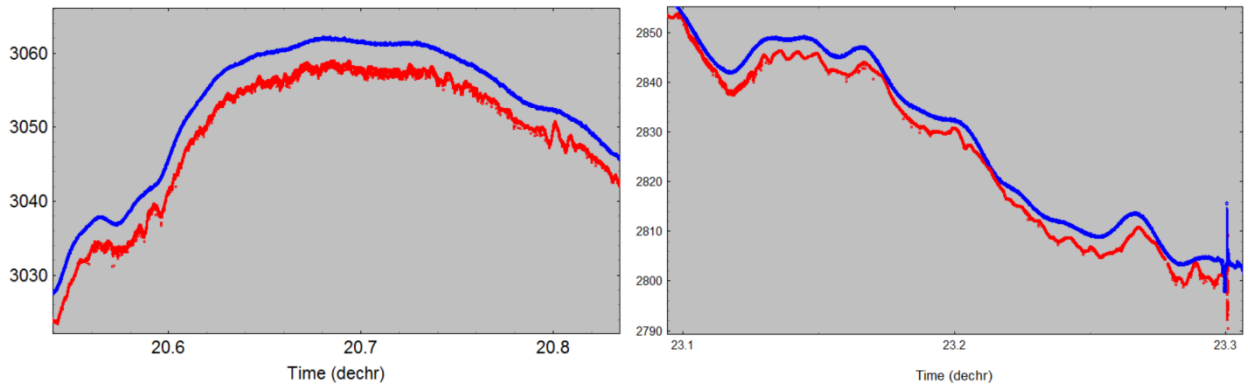

Fig. 20. Examples of retracked ASIRAS data on the outbound (from pole) and inbound tracks. The spikes at the far right represent the overflight of the Amundsen-Scott South Pole station building. The inbound flights retracked data are affected by out-of-window radar range data, which may disturb OCOG results, and are likely the sourse of the non-consistent offsets in this part of the flight.

Table 4. *Ellipsoidal heights of the South Pole station roof*
(the overflight passed over the left side wing, shown in picture insert)

Height from GPS (ITRF)	2815.53 m
Height from lidar	2815.47 m
Height from ASIRAS	2809.14 m

7. MAGNETIC DATA PROCESSING

The aeromagnetic data for the PolarGap survey were collected on an opportunistic basis, and will contribute towards filling the major data void in the South Pole region that still remains in the latest international Antarctic-wide magnetic data compilation ADMAP2.0. The data were collected with Scintrex Cesium Cs3 magnetometers, mounted on the aircraft wing tips. An initial correction accounted for DC offsets caused by the aircraft tip tanks. No dedicated survey flight was flown to calculate standard magnetic compensation coefficients, which are typically required to then correct for aircraft motion effects. Therefore, to minimize aircraft-induced magnetic noise the 10 Hz total field line data were filtered with a low pass filter (150 samples equal to ~900 m). Following this "pseudo-magnetic compensation" procedure, the magnetic dataset was decimated to 1Hz. Standard magnetic heading corrections have so far not been applied, as these were deemed to be better accounted for during advanced leveling processes (not described here). To correct the total field magnetic data for core field effects we adopted the 2015 IGRF, using the provisional IGRF coefficients provided in the commercial software "Geosoft". The IGRF reference field was calculated at the survey line elevation and at the appropriate date during which the line was flown.

Aeromagnetic surveys in the polar regions are adversely affected by strong diurnal magnetic field variations induced by solar activity. Diurnal corrections were therefore applied using data from a suite of fixed magnetic base stations. Data from total field sensors at FD83 and Thiel Mountains, along with total field variations calculated from a fluxgate system at South Pole show that survey flights were generally flown in relatively magnetically quiet periods of the day. However, some flights were flown in non-ideal noisy conditions, and for these flights the overall quality of the processed aeromagnetic anomaly data is therefore relatively lower, cf. Fig 21.

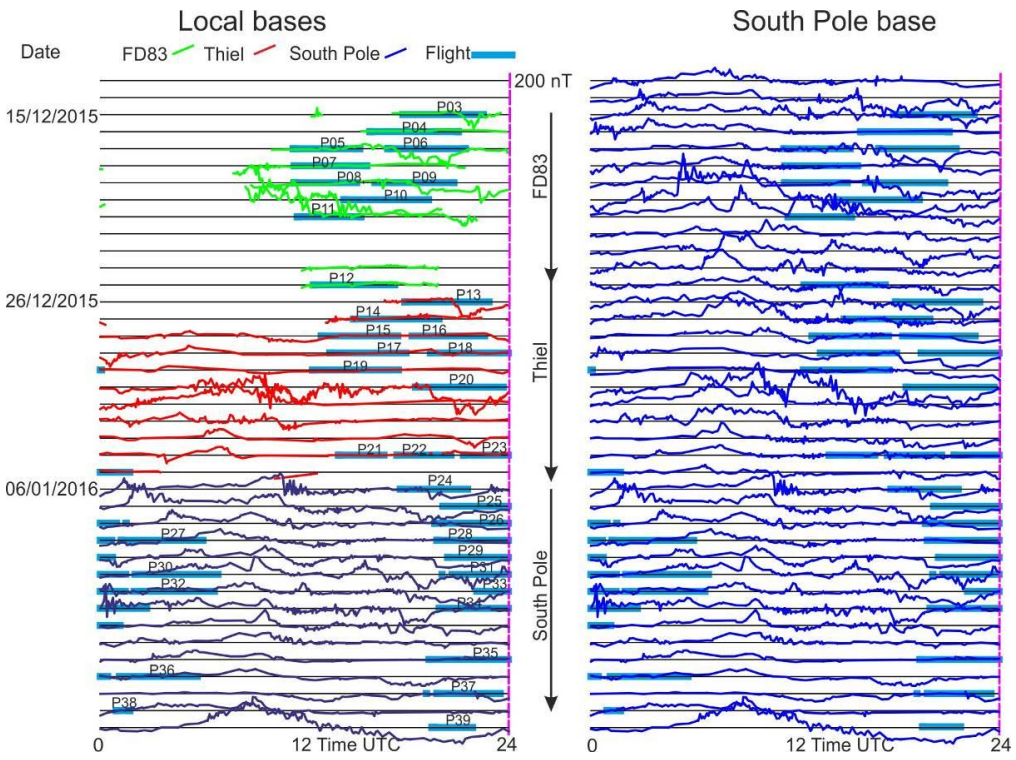

Fig. 21. Variations in the external magnetic field, as measured from mag base stations. Note the blue lines and labels (P03-P39) that show the duration of the individual survey flights. Left panel shows 'local' base stations at FD83, Thiel and South Pole, while right panel shows the South Pole station data alone.

To further improve our diurnal correction for the PolarGAP aeromagnetic dataset we also considered additional data from fluxgate magnetometers forming part of the Penguin network (Fig. 22). Due to the Earth's deep electrical conductivity the spatial pattern of the diurnal correction can vary significantly (both in terms of amplitude and phase) over such a large survey area and hence using more magnetic base stations can be helpful in reducing potential biases both within and between different survey flights.

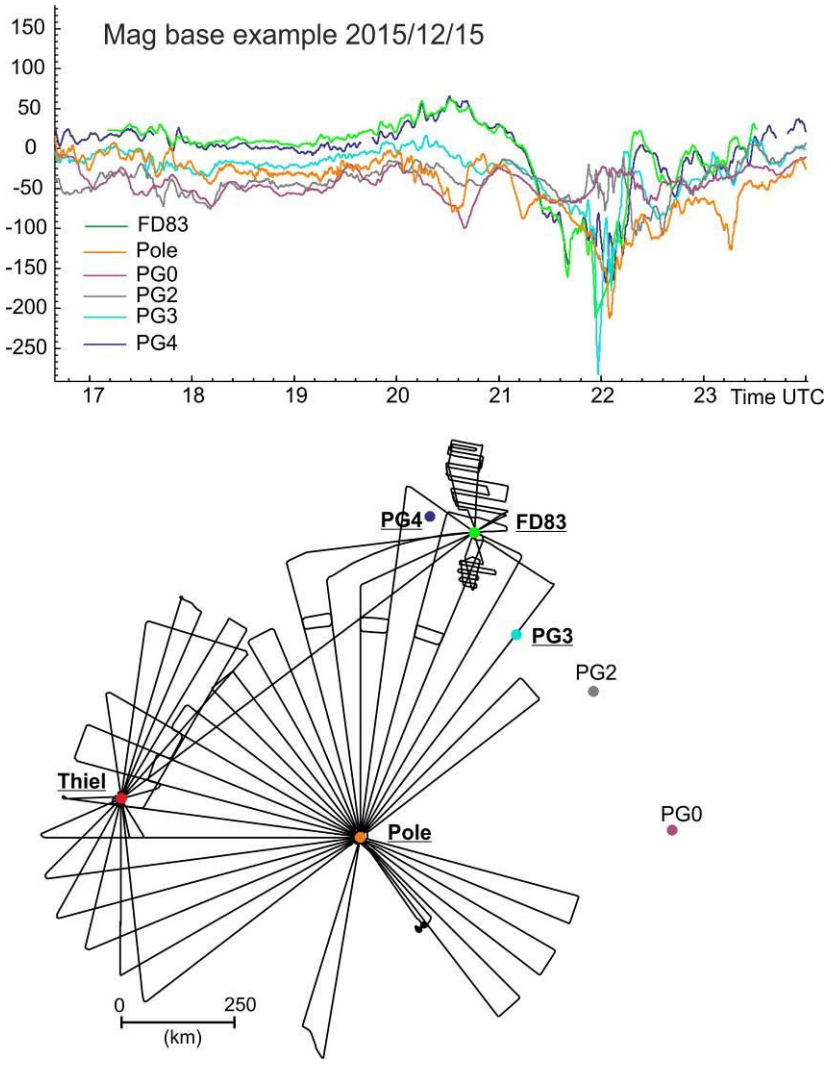

Fig 22. Top: Example of total field base station data from FD83, compared with data from fluxgate stations forming part of the Penguin network PG0-PG4, and South Pole. Note that stations PG0 and PG2 do not appear to correlate well with the FD83 station and were therefore excluded from the Inverse Distance Weighting calculation adopted for the final diurnal correction processing step.

To provide an enhanced diurnal correction we implemented an Inverse Distance Weighting (IDW) technique to integrate data from all available base stations in the survey region. This was particularly important for flights that started at one field site, but ended at another. Fig. 23 shows two examples of this correction.

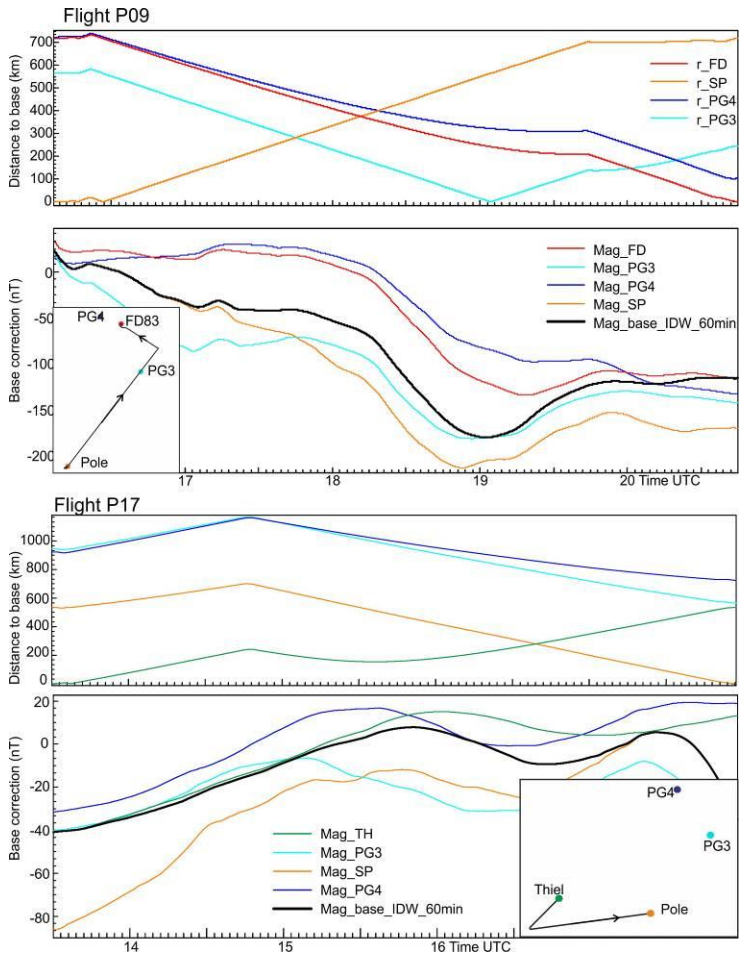

Fig. 23. Local base station values (coloured lines) and calculated Inverse Distance Weighting (IDW) diurnal corrections.

It is important to note that short wavelength diurnal variations observed at a base station are often not fully representative of those occurring at large distances from the base station (therefore typically for distances over 100 km from the base station the correction data have to be filtered). Base station data were filtered with a 60 minute and 30 minute filter prior to the inverse distance weighting. The influence of the base station correction on the aeromagnetic data is shown in Fig 23. Using filtered diurnal corrections calculated with the IDW method leads to a significantly reduced line to line residual corrugation and hence an improved quality of the aeromagnetic anomaly data (compare fig. 23a and fig. 23d). Additionally, cross over errors at line intersections are reduced from RMS values of ca 143 nT prior to base station correction (Fig. 23a), to approximately 90 nT when using a single filtered magnetic base station correction dataset at South Pole (Fig. 23b), and to 47 nT and 52 nT (30 min and 60 min filters respectively), when applying multiple filtered magnetic base station data and the IDW method (figs. 23c & d).

We note that the cross-over errors appear to be slightly lower for a 30 minute filter compared to the 60 minute filter. However, in most large-scale Antarctic aeromagnetic surveys to date e.g [RD 9, 10] a 60 minute filter has proven to be an ideal compromise between applying a representative long-wavelength diurnal correction to the line data and then accounting for higher frequency residual diurnal variations with tie line levelling. In accordance with processing parameters for previous large-scale surveys we therefore adopt a 60 minute filter as our preferred choice (fig. 24).

Figure 25 shows the final aeromagnetic anomaly dataset after tip tank corrections, low-pass filtering (as a proxy for magnetic compensation), IGRF correction and IDW magnetic base station corrections. Levelling has so far not been applied to these aeromagnetic data as the final levelling process will require integration of the new PolarGAP aeromagnetic line data with previous aeromagnetic survey datasets within the study region, in order to increment both the number and the overall reliability of cross-over data [see e.g. RD11].

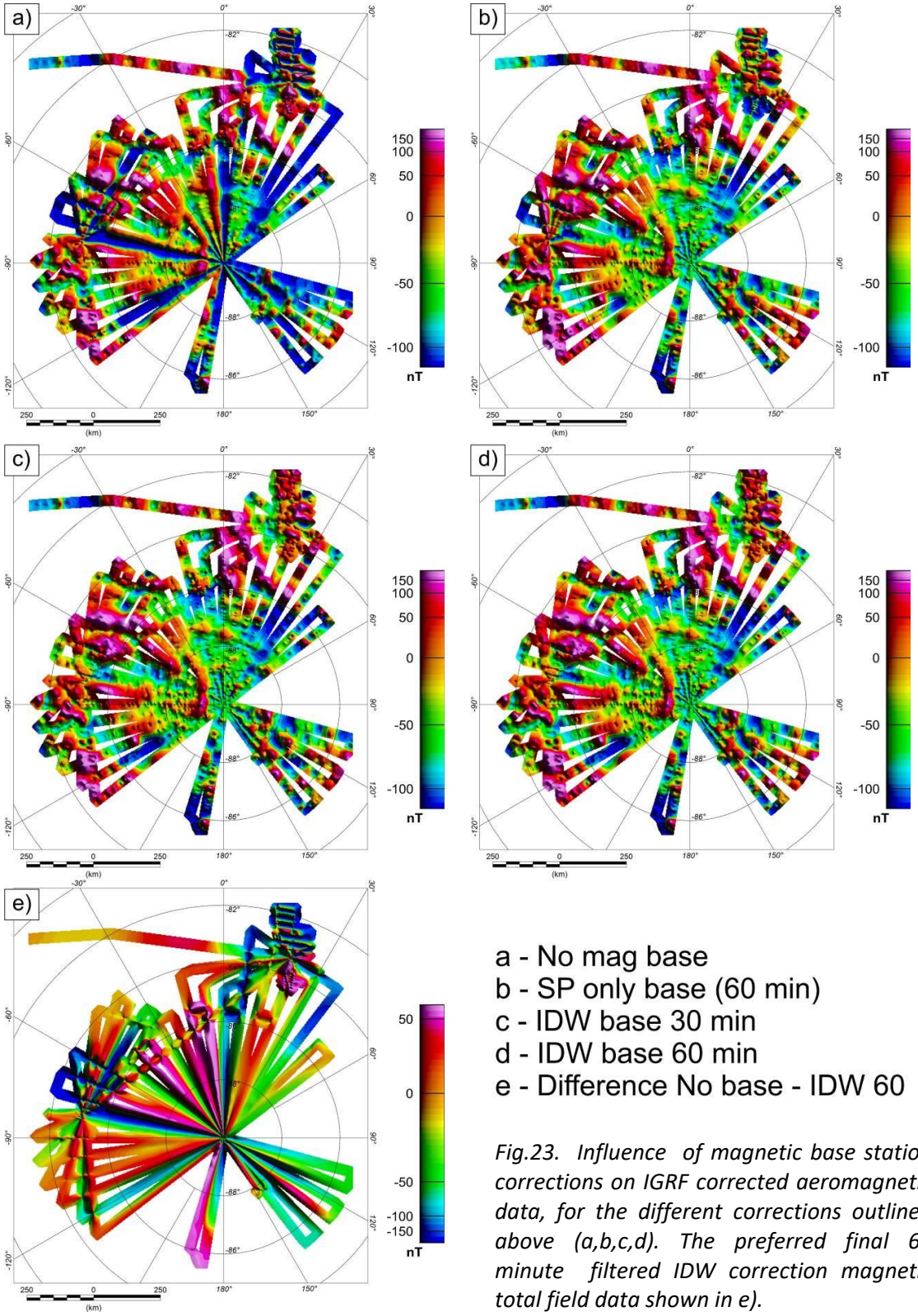

Fig.23. Influence of magnetic base station corrections on IGRF corrected aeromagnetic data, for the different corrections outlined above (a,b,c,d). The preferred final 60 minute filtered IDW correction magnetic total field data shown in e).

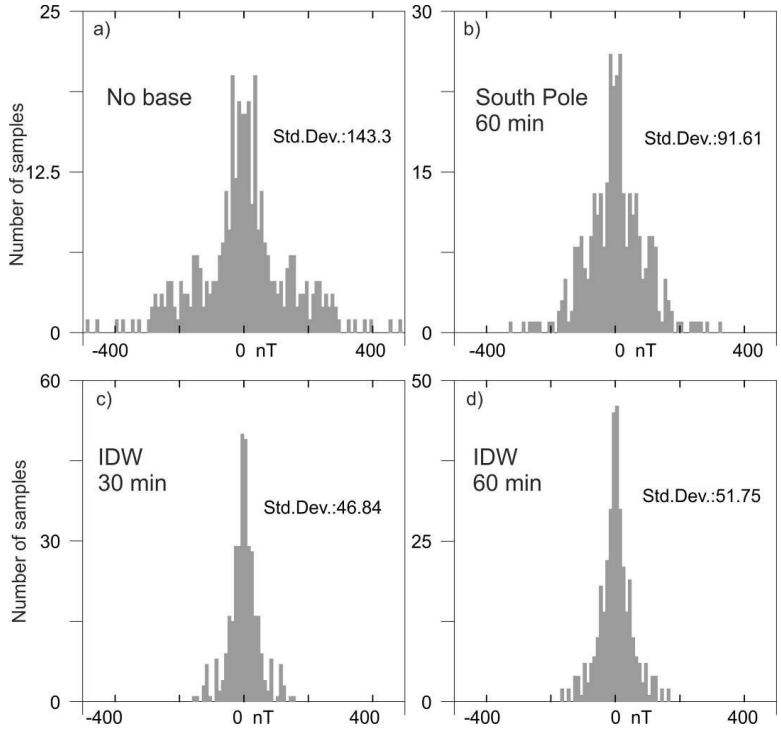

Fig 24. Histogram analysis showing errors for no base station correction, South Pole only correction, and with IDW base station corrections with 30 and 60 minute filters respectively. Note the significantly lower standard deviation in errors at cross-overs obtained after applying the IDW filtered base corrections.

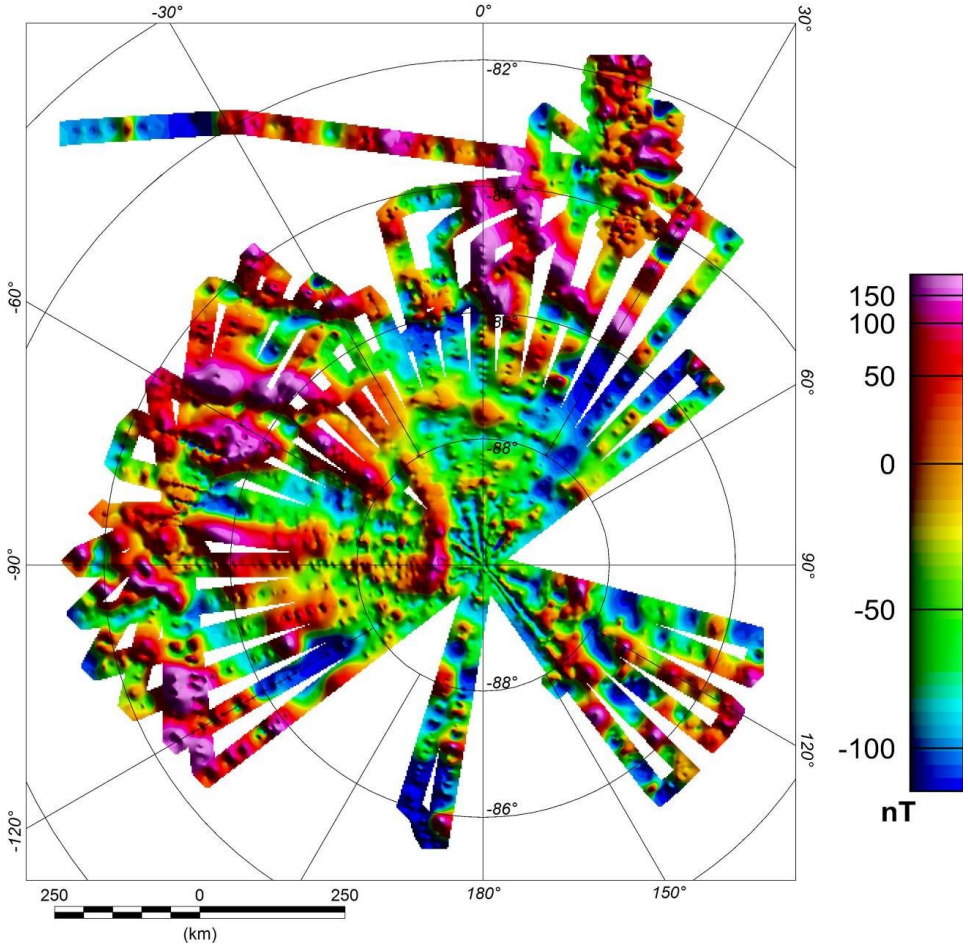

Fig. 25. Final PolarGAP aeromagnetic data with 60 min IDW filtered diurnal correction applied.

8. ICE-PENETRATING RADAR PROCESSING

The 150 MHz BAS ice-sounding radar was flown throughout the survey [RD12]. Although the radar data were collected on an opportunistic basis, it will provide a key dataset for ongoing Antarctic geosciences investigations in the South Pole region. In addition, the sub-ice topography is vital for correcting the new PolarGAP free-air gravity anomalies for ice thickness and topography, and hence obtain the fully terrain corrected Bouguer gravity anomalies used for subsequent geophysical studies of the region.

An unfocused SAR processing scheme with Doppler beam sharpening was performed to enhance the signal to clutter ratio of the bed echo and improve visualisation. The received chirp of 4 µs, 12 MHz bandwidth data was compressed, filtered, and decimated from the original trace acquisition rate of 156.25 Hz to 2Hz, equivalent to ~30m in along-track spacing. These data, with a range sampling of 24 MHz were converted to a SEGY format for further processing. After optimised gain correction a semi-automated 'first break' process applied within the seismic processing package ProMax was used to identify the onset of the bed echo. Subsequent manual editing was used to remove spurious results of the automated picker and identify bed reflections in areas with very low bed return power.

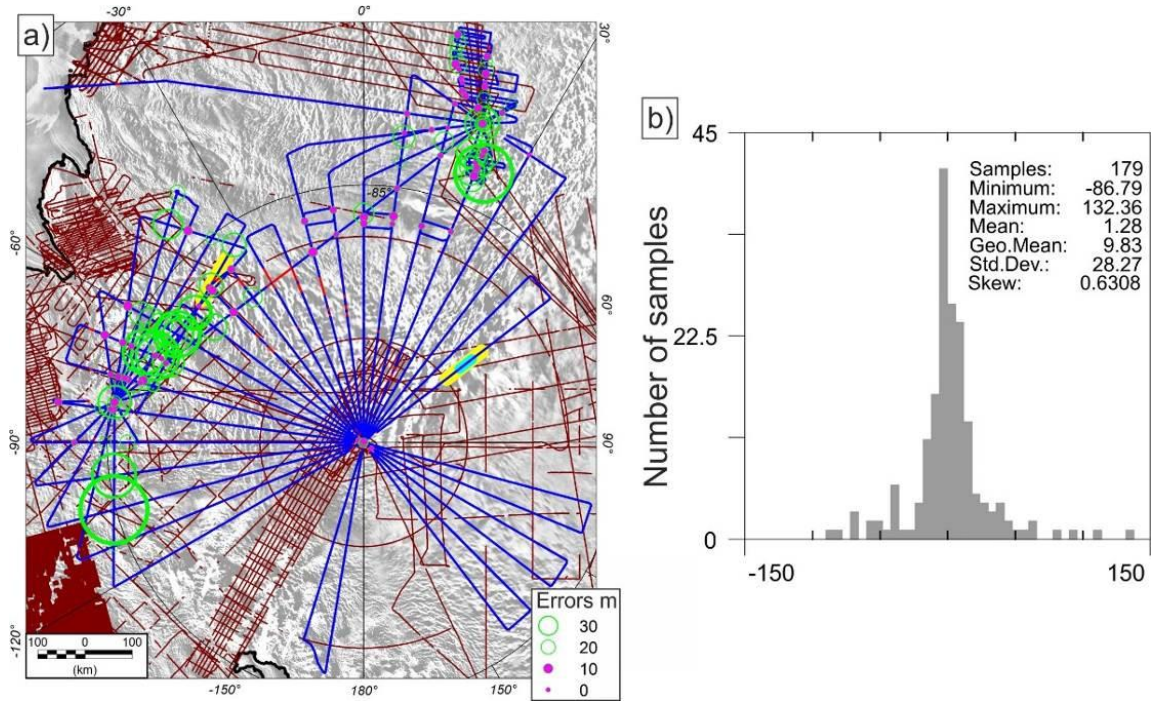

Fig. 26. Radar data coverage and uncertainties. a) New PolarGap radar data location (dark blue lines). Bright red line segments mark regions where no bed pick was resolved. Brown lines mark pre-existing Radar surveys including SPRI/NSF/TUD, Dufek, CAZERTZ, Pensacola Pole Traverse, AGAP, Institute AFI, ICEGRAV 2013, and the ongoing ICEBRIDGE mission. Yellow sections mark profiles in Fig. 8.3. Pale blue section marks a previously un-reported subglacial lake. Green circles show crossover errors, filled circles indicate errors <10m. b) Histogram of crossover errors.

Where possible, the ice surface location within the radargrams was calculated using lidar measurements of surface elevation. In areas where lidar data was not available the location of the surface reflection was picked directly from the radargram and a regression, local to the data

gap, was used to fit the radar range to terrain clearance. Ice thickness (m) was calculated from the picked bed location and theoretical (or picked) surface location.

An EM velocity of Vice = 168 μsm^{-1} was taken to convert the range delay to ice thickness; a standard firn correction of 10m was also added. The Ice bed elevation (m) was calculated by subtracting ice thickness from the surface elevation. Bed elevation was integrated with a high precision kinematic dual-frequency GPS position solution to provide the final point data set of ice thickness and bed elevation relative to WGS84. Although some data gaps are present bed reflections were resolved along 95.5% of the radar profiles (Fig. 26a). Crossover analysis of recovered bed elevation across the entire survey gives an error estimate for the PolarGAP survey of ~28 m (Fig. 26b).

The final gridded datasets (Appendix 2) reveal several regions with ice thickness over 3250 m in the interior of the ice sheet (Fig. 27a). When converted into a map of bed elevation the deep Pensacola Pole Basin, extending from the coast to South Pole is clearly imaged (Fig. 27b). In addition, internal ice sheet layers and subglacial lakes are resolved (Fig. 28).

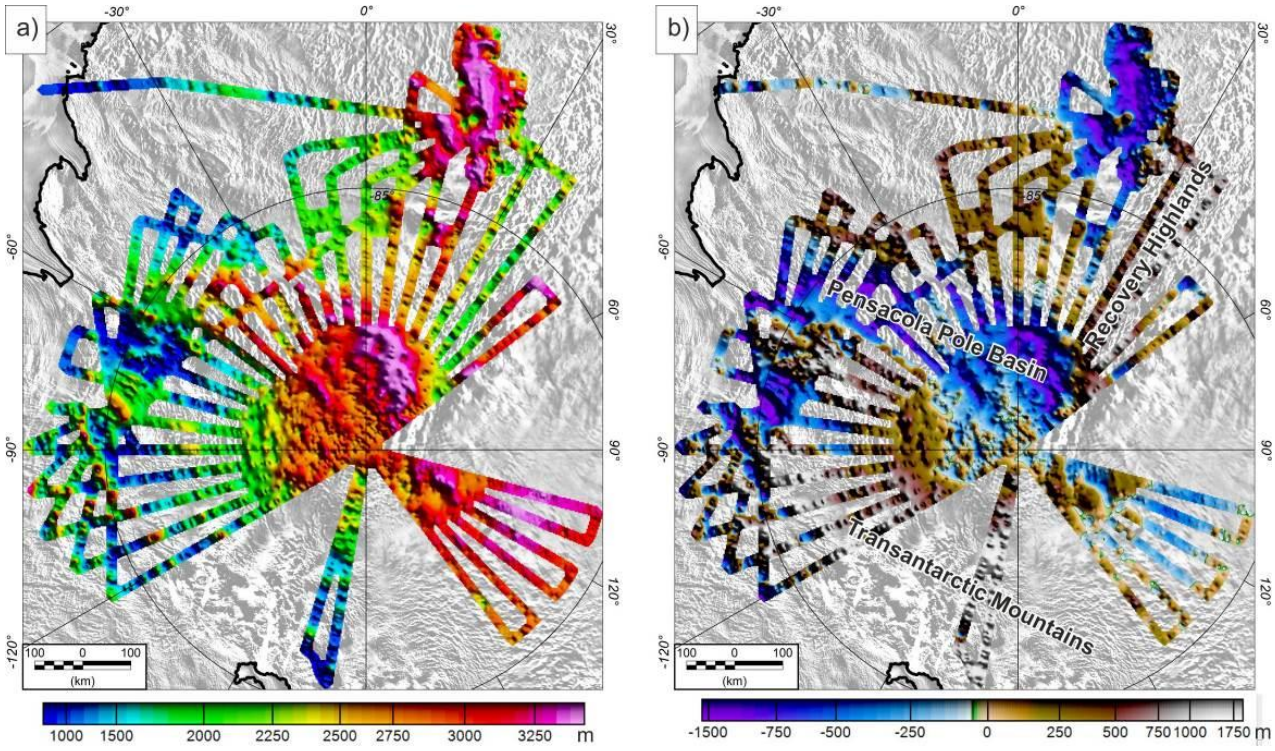

Fig. 27. PolarGAP ice thickness (a) and bed elevation (b).

A preliminary compilation of the PolarGAP radar data with other surveys in this region provides a new view of the subglacial topography (Fig. 29). The new detail is highlighted by comparison with the existing BEDMAP2 data set [RD13] (Fig. 29a). Differences are generally in the order of +/-450m in many regions (Fig. 28c). However, local differences of as much as -2.5 km are seen in incised valleys west of Thiel Mountains, and +1.6 km over isolated buried nunataks are seen along profiles.

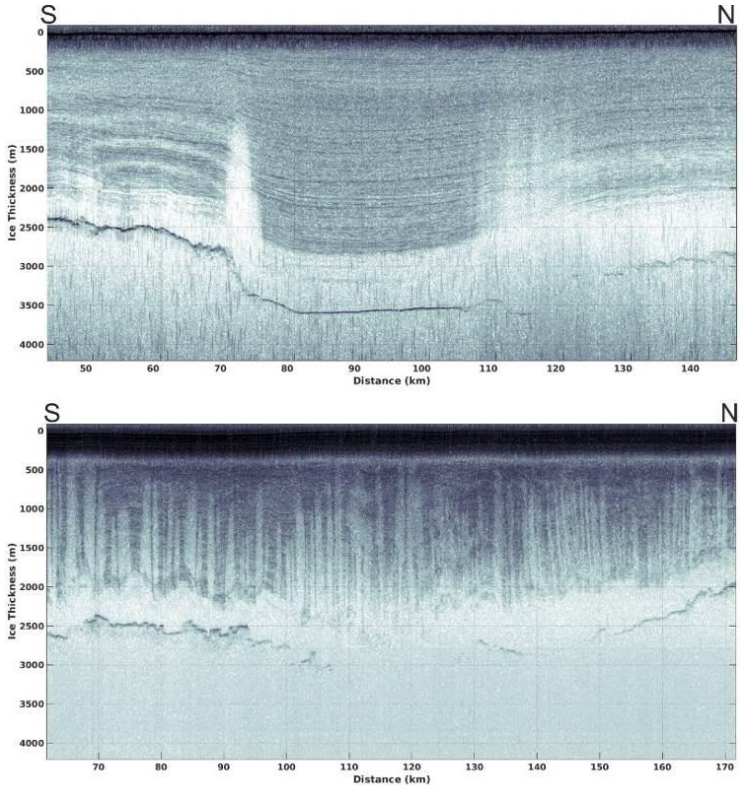

Fig. 28. Examples of Radar data. a) Section over previously unreported ~22 km wide subglacial lake in a region of slow (~3m/a) ice flow. Note well resolved bed along ~99% of the profile. Also note well defined and continuous internal layers. b) Section over the Pensacola-Pole Basin with ice flow of up to 79 m/a. Bed is recovered along ~85% of this profile. Note disrupted and buckled internal layers.

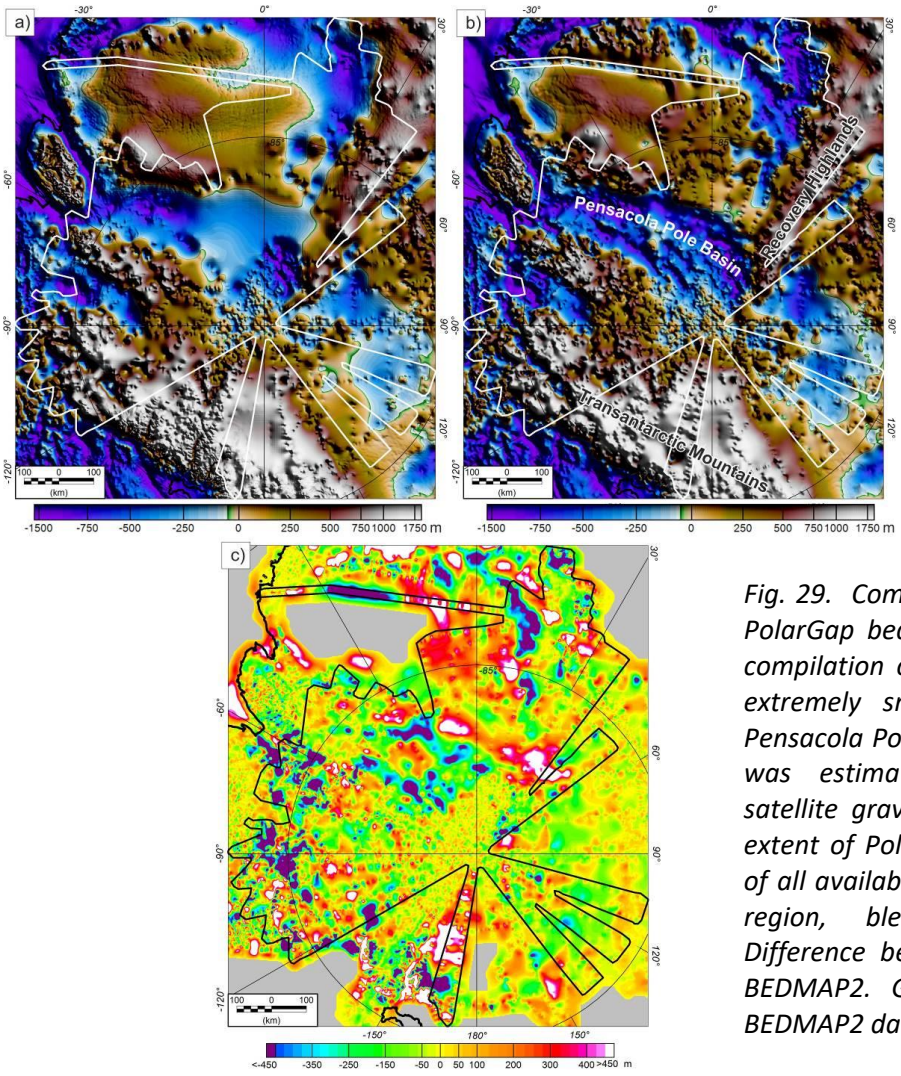

Fig. 29. Comparison of BEDMAP2 with new PolarGap bed elevation data. a) BEDMAP2 compilation of subglacial topography. Note extremely smooth regions, including the Pensacola Pole Basin where bed topography was estimated using long wavelength satellite gravity data. White outline shows extent of PolarGap data. b) Integrated grid of all available radar data in the South Pole region, blended with BEDMAP2. c) Difference between new blended grid and BEDMAP2. Grey areas show where only BEDMAP2 data was used.

ACKNOWLEDGEMENTS

The PolarGap team thank NSF for access to South Pole Station, fuel support, and transit from/to South Pole to Christchurch, New Zealand via McMurdo; we thank the staff at South Pole station for kind and efficient support. Norsk Polarinstitut and the staff at Troll are thanked for their logistic support for the project, ALE for permission to use fuel at the Thiel Mts depot, and ALCI for timely provision of logistics services. We thank professor M. Becker, TU Darmstadt, for providing the iMAR RQH-1003 for the project. We thank Kevin Hughes from the BAS environmental office and Polly Penhale from NSF for helping arrange flights through the South Pole ASMA.

David Becker, TU Darmstadt, carried out the iMAR processing for both attitude and IMU gravity of the PolarGap project. Fientje Kasenda, DTU Space, processed most of the GPS and lidar data. Hasan Yildiz, General Command of Mapping, Turkey, provided support for the upward continuation of gravity gradients by least-squares collocation. Veit Helm, AWI, processed the raw L1 ASIRAS data, and Graeme Eagles, AWI, provided the Dome-C and RECISL raw gravity data for final DTU aerogravity processing. Kirsty Tinto, LDEO, Columbia University, provided two key profiles from the ongoing ROSETTA Ross ice shelf gravity and bathymetry project. Sam Seddon, BAS provided assistance in digitizing radar data. Henriette Skourup and Tim Jensen, DTU Space, provided assistance in retracking ASIRAS data.

REFERENCE DOCUMENTS

[RD1]: PolarGap 2015/16: Filling the GOCE Polar Gap in Antarctica, Data Acquisition Report, version 4, June 2016.

[RD2]: Olesen, A.V.: Improved airborne scalar gravimetry for regional gravity field mapping and geoid determination. National Survey and Cadastre of Denmark, Technical Report 24, 123 pp., 2002.

[RD3]: Becker, D, Nielsen, JE, Ayres-Sampaio, D, Forsberg, R, Becker, M & Bastos: Drift reduction in strapdown airborne gravimetry using a simple thermal correction, Journal of Geodesy, vol. 89, no. 11, pp. 1133-1144, 2015, doi:10.1007/s00190-015-0839-8.

[RD4]: Forsberg, R., A. V. Olesen, F. Ferraccioli, T. A. Jordan, K. Matsuoka, A. Zakrajsek, M.Ghidella and J. S. Greenbaum: Exploring the Recovery Lakes region and interior Dronning Maud Land, East Antarctica, with airborne gravity, magnetic and radar measurements. Geol. Soc., London, Special Publications, 461, 20 Sep 2017, https://doi.org/10.1144/SP461.17.

[RD5]: Scheinert, M., F. Ferraccioli, J. Schwabe, R. Bell, M. Studinger, D. Damaske, W. Jokat, N. Aleshkova, T. Jordan, G. Leitchenkov, D. D. Blankenship, T. M. Damiani, D. Young, J. R. Cochran, T. D. Richter: New Antarctic gravity anomaly grid for enhanced geodetic and geophysical studies in Antarctica. Geophysical Research Letters, 43(2), 600-610, doi:10.1002/2015GL067439, 2016.

[RD6]: Tscherning, C. C., R. Forsberg and P. Knudsen: The GRAVSOFT package for geoid determination. Proc. IAG first continental workshop for the geoid in Europe, Praque, pp. 327-334, 1992.

[RD7]: Forsberg,R, A V Olesen, F Ferraccioli, T A Jordan, K Matsuoka, A Zakrajsek, M Ghidella and J S Greenbaum: Exploring the Recovery Lakes region and interior Dronning Maud Land, East

Antarctica, with airborne gravity, magnetic and radar measurements. Geological Society, London, Special Publications, 461, 2017, https://doi.org/10.1144/SP461.17.

[RD8]: Steinhage, D., G. Eagles, R. Forsberg, H. Yildiz: Dome-C airborne gravity measurements and comparison to GOCE gradient data. DTU Space/ESA campaigns office, DEC 2013.

[RD9]: Ferraccioli, F. Armadillo, E. Jordan, T., Bozzo, E., Hugh Corr: Aeromagnetic exploration over the East Antarctic Ice Sheet: a new view of the Wilkes Subglacial Basin, Tectonophysics, 478 (1), 62-77.

[RD10]: Ferraccioli, Finn, C.A., Jordan, T.A., Bell, R.E., Anderson, L.M., Damaske, D.: East Antarctic rifting triggers uplift of the Gamburtsev Mountains, Nature, 479, 7373, 388-392.

[RD11] Aitken, A.R.A., Young, DA, Ferraccioli, F, Betts, PG, Greenbaum, JS, Richter, TG, Roberts, JL, Blankenship, DD, Siegert, MJ, The subglacial geology of Wilkes Land, East Antarctica, Geophysical Research Letters, 41 (7), 2390-2400.

[RD12]: Corr, H., F. Ferraccioli, N. Frearson, T. A. Jordan, C. Robinson, A. Armadillo, G. Caneva, E. Bozzo and I. E. Tabacco (2007). Airborne Radio-Echo Sounding of the Wilkes Subglacial Basin, the Transantarctic Mountains, and the Dome C Region. The Italian–British Antarctic Geophysical and Geological Survey in Northern Victoria Land 2005–06—Towards the International Polar Year 2007–08. E. Bozzo and F. Ferraccioli, Terra Antartica Reports. 13: 55-63.

[RD13]: Fretwell, P., et al., (2013). "Bedmap2: improved ice bed, surface and thickness datasets for Antarctica." The Cryosphere 7(1).

PolarGap Recovery Lakes field camp, organized by NPI

APPENDIX 1. OVERVIEW OF FLIGHTS

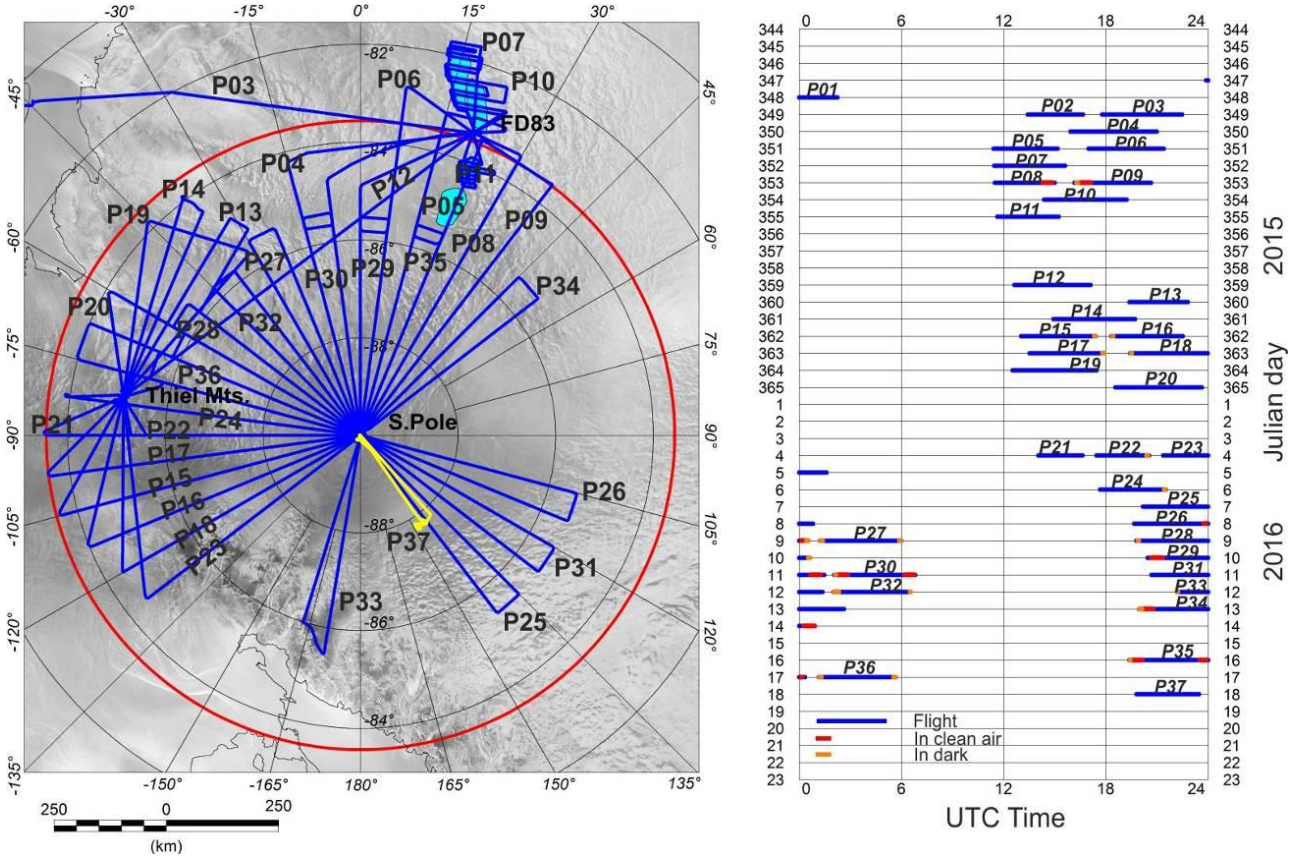

PolarGAP flight overview. Left: Map of PolarGAP gravity flights (blue) numbered in the order flown (P03 to P36). Yellow line marks the ASIRAS flight (P37) over the CryoSat elevation change anomaly. Right: Graphic showing survey progress in time. The primary data reference for flight days are either Julian Day (JD) or survey flight number (P01-P38). Red and orange sections on the figure show time of flights through normally restricted Clean Air, and Dark sectors of the South Pole SCAR Specially Managed Area (ASMA #5).

The survey team at the South Pole, after the last PolarGap flight on JAN 19, 2016.

APPENDIX 2. DATA DOWNLOADS

Gravity

Final PolarGap gravity results are in ASCII files of line format: line_no*10000+running no, latitude, longitude, ellipsoidal height, and gravity disturbance (mgal), time (Julian Day). The files are stored in
ftp2.spacecenter.dk/pub/avo/ANTARCTICA/GRAVITY/polargap-may2017_gravity.zip

The gravity disturbance file has extension ".dg", free-air anomaly file ".fa" (using the GOCE R5 geoid for conversion).

Gravity gradient data can similarly be downloaded from
ftp2.spacecenter.dk/pub/avo/ANTARCTICA/GRADIENTS/polargap_trf_neu_gradients.zip

The files include the individual gravity gradients predicted at 225 km or 255 km heights by collation. The format is id, lat, lon, height, predicted gradient and error estimate in Eotvos. Some additional auxillary plot files are included as well.

Lidar

A 5x5 thinned/cross-track averaged version of the lidar data can be downloaded from
ftp2.spacecenter.dk/pub/avo/ANTARCTICA/LIDAR/5x5_ZIP/.

The non-thinned 1-m resolution files are rather big, 4 GB pr flight, and are available on request. Contact: Fientje Kasenda, afk@space.dtu.dk.

ASIRAS

The OCOG retracked ASIRAS data are available, along with some at
ftp2.spacecenter.dk/pub/avo/ANTARCTICA/ASIRAS/polargap_asiras_files.zip

The AWI processed L1B ASIRAS data are available on request to Henriette Skourup,
hsk@space.dtu.dk

Magnetics

Aeromagnetic data is provided as a 1Hz comma separated ASCII file and as a Geosoft database. In ASCII file "No data" = *. Data channels and processing scheme follows the ADMAP naming convention and is laid out in the table below.

Aeromagnetic and magnetic base station data is available from:
ftp://ftp.bas.ac.uk/tomj/PolarGAP/PolarGAP_mag_distro.zip

Aeromagnetic data.

PolarGAP_mag_ADMAP_ASCII.zip & PolarGAP_Mag_1Hz_post_proc_split_ADMAP.gdb

Channel name	Description
Line No./Flight No.	PXX.Y, where XX is flight number, and Y is part of flight **Example:** P05.2
LON	Longitude (degrees). For flights P03 to P38 this is differentially processed kinematic GPS position, while P39 uses the 'raw' position recorded during the flight. NOTE magnetic data was recorded before kinematic GPS data so dummies may exist in the navigation channels.
LAT	Latitude (degrees). Processed as for Longitude.
ELEV	Flight elevation (meters). Elevation with respect to the WGS1984 ellipsoid (processed as for Longitude).
DATE	Date in time format. **Example:** 2015/12/15
TIME	UTC time **Example:** 22:09:06
MagR	The raw magnetic observation (nT). **Example:** 50070.2
MagC	Compensated MagR (nT). No compensation was applied due to survey design, so a 15 second (~900 m) low pass filter was used to minimise short wavelength noise correlated with aircraft motion as seen on three axis fluxgate data. NOTE correction was calculated by filtering 10 Hz tip corrected data, then re-applied to MagR. **Example:** 50068.5
Tcorr	Tiptank correction (nT) and dummy values at jumps or before take off. **Example:** -150
RefField	Geomagnetic reference field value (nT). IGRF calculated in Geosoft using date field and IGRF 2015. **Example:** 50166.1
MagRTC	This is the compensated magnetic value adjusted for the Tiptank and geomagnetic field values. (MagRTC) = (MagC) + (Tcorr) – (RefField) **Example:** -96. 1
Bcorr	Diurnal correction (nT). Calculated using an inverse distance weighting of all available 60 minute filtered base station data. See separate database/table for individual raw base station corrections. **Example:** -83.7
MagBRTC	(MagBRTC) = (MagRTC) – (Bcorr) **Example:** -12.2
Scorr	Additional mask channel. Used to remove data at start/end of flights where multiple lines converge. 0 = use, dummy = remove.

MagF	Final mag value (nT) after all corrections and prior to levelling. (MagF) = (MagBRTC) + (Acorr) + (Scorr) **Example:** -12.2

Magnetic base station data.

Magnetic base station data came from a range of sources, including total field sensors set up at field camps and fluxgates deployed as part of the Polar Experimental Network for Geospace Upper atmosphere Investigations (PENGUIn)/AAL-PIP geomagnetic observatory network. Station details are in the table below. The Antarctic AAL-PIP data have been provided by Virginia Tech which is supported by the National Science Foundation through the following awards for this purpose: ANT0839858, ATM922979, ANT0838861, PLR-1243398, and PLR-1543364.

Station Name	Lon	Lat	Elevation	Mean field	Raw data type	Sensor description and operator
FD83	20.5469	-83.3993	2613.766	50283.508	Total field nT	Cesium vapour (DTU).
Thiel	-80.7732	-85.0861	1352.650	53031.61	Total field nT	Proton procession (BAS)
Pole	-0.19297	-90	2797	54828.29	three axis voltage	Lucent Technologies fluxgate (PENGUIn).
PG3	37.62937	-84.8101	3115.847	52138.13	Three axis nT	Korepanov Fluxgate Magnetometer (PENGUIn).
PG4	12.25265	-83.3399	2538.952	49993.43	Three axis nT	Korepanov Fluxgate Magnetometer (PENGUIn).

Total field values for the various base stations used, along with calculated inverse distance weighted (IDW) diurnal correction values are provided as a comma separated ascii file and as a geosoft database. Note base station data is only provided for time coincident with flights. Base station channels are described in the table below. Files: Mag_base_IDW_Distro.zip & Mag_base_IDW_Distro.gdb

Channels	Description
TimeUTC,UTCDate	Time and date values
Longitude,Latitude,x,y	Aircraft navigation data (geographic and projected)
power	Coefficient used in IDW calculation
Mag_base_Thiels,Mag_TH_fill_30,Mag_TH_fill_60	Raw, 30 minute and 60 minute filtered data from Thiel base station. NOTE for 30 and 60 minute channels dummies are replaced with zero.
Mag_base_FD83,Mag_FD_fill_30,Mag_FD_fill_60	Raw, 30 minute and 60 minute filtered data from FD83 base station. NOTE for 30 and 60 minute channels dummies are replaced with zero.
Mag_base_PG3,Mag_PG3_30min,Mag_PG3_60min	Raw, 30 minute and 60 minute filtered data from PG3 base station.
Mag_base_PG4,Mag_PG4_30min,Mag_PG4_60min	Raw, 30 minute and 60 minute filtered

	data from PG4 base station.
Mag_base_SP,Mag_SP_30min,Mag_SP_60min	Raw, 30 minute and 60 minute filtered data from South Pole base station.
r_FD,r_TH,r_PG3,r_PG4,r_SP	Range in m to each base station. Note when FD83 or Thiel are dummies range is set to 10,000 km
Mag_base_IDW_30min,Mag_base_IDW_60min	IDW combination of filtered base station data (30 or 60 minute).

Ice-penetrating Radar

PolarGAP radar data is provided as 2.5 km cell size rasters of ice thickness and bed elevation. Point data was interpolated using a tensioned spline method with an internal tension of 0.25.

Radar grids are available from:
ftp://ftp.bas.ac.uk/tomj/PolarGAP/PolarGAP_radar_grids.zip

Data is provided in two formats (netCDF and ASCII):

1/ Polar stereographic projected netcdf grids (.nc files), with true scale at -71 and a central meridian of zero.
Files are: PolarGAP_tice_2.5km.nc and PolarGAP_bedelev_2.5km.nc

2/ Compressed ASCII comma separated table with Longitude, Latitude, ice thickness and bed elevation. Areas of no PolarGAP data are represented by NaN.
File: PolarGAP_2.5km_ASCII_grid.zip